Mon. Not. R. astr. Soc. (1992) **257**, 317–339

Distances for galactic planetary nebulae using mean [O II] doublet ratio electron densities

Robin L. Kingsburgh and M. J. Barlow
Department of Physics and Astronomy, University College London, Gower Street, London WC1E 6BT

Accepted 1992 January 30. Received 1992 January 28; in original form 1991 November 22

SUMMARY

We present [O II] 3726, 3729-Å doublet ratios and electron densities for 68 galactic planetary nebulae (PN). For 45 of the objects, the doublet ratios represent integrations over the whole of the nebula. Distances have been derived for the majority of the nebulae, using calibrations recently derived from Magellanic Cloud PN. For PN which are optically thin in the hydrogen Lyman continuum, we have derived distances using a variant of the Shklovsky method (constant ionized hydrogen mass) which uses the mean [O II] electron density and the measured radio flux and which does not require knowledge of the filling factor or nebular angular radius. For PN which are optically thick in the Lyman continuum, the constant Hβ flux method was used to derive distances. The typical [O II] density at the transition point between an optically thick and thin nebula is 4500 cm^{-3}. Since the optically thin and thick methods both overestimate the distance when applied to inappropriate nebulae, the smaller of the two distance estimates is adopted for each nebula. An extensive comparison is made between the distances derived here and previously published distances and distance scales. It is shown that the present distances, based on Magellanic Cloud calibrations, give consistency with independent distance estimates. They also yield much greater self-consistency between central star masses derived from luminosity versus $T_{\rm eff}$ comparisons on the one hand, and from absolute magnitude versus evolutionary age comparisons on the other hand. For the PN in our sample, rms electron densities, filling factors and absolute radii have also been derived. The derived filling factors are found to decrease with increasing absolute angular radius, but we argue that this effect can be attributed entirely to the effects of measurement uncertainties in the adopted angular radii.

Key words: planetary nebulae: general.

1 INTRODUCTION

One of the outstanding problems in the study of galactic planetary nebulae (PN) is the lack of a well-calibrated distance scale, since knowledge of the distances to PN is crucial for studies of the evolution of the central stars and their surrounding nebulae. Once the distance to a PN is known, various nebular and central star parameters can be established, including the central star effective temperature and luminosity, thereby allowing comparisons to evolutionary models to be made. Distances to PN also enable their galactocentric positions and scaleheights to be calculated, essential for the study of the interstellar medium (ISM) enrichment rate; PN are believed to be the prime producers of carbon and important producers of nitrogen for the interstellar medium.

Distances to small numbers of individual PN have been derived by a number of methods, including binary or cluster membership, dust extinction versus distance (e.g. Gathier, Pottasch & Goss 1986b), H I absorption radial velocity distances (e.g. Gathier, Pottasch & Pel 1986a), and the determination of log g and $T_{\rm eff}$ for absorption-line central stars followed by distance calibration via comparison with model evolutionary tracks (e.g. Mendez *et al.* 1988).* For distances to a larger sample of PN, one must turn to 'statistical' methods which can be calibrated by PN having known distances (e.g. Cahn & Kaler 1971; Daub 1982) or by using statistical parallaxes (e.g. Cudworth 1974). These statistical methods rely on the basic premise that most PN have evolved in a similar way from similar progenitor stars. The

* Lutz (1989) reviews these methods.

standard assumption is that a PN is initially optically thick to H I Lyman continuum radiation. As the nebula expands and its density drops, the ejected material eventually becomes fully ionized and the PN becomes optically thin. Later, when the luminosity of the central star drops, full ionization of the nebula may cease; the PN may again become optically thick. For a PN in the optically thin stage, the distance can be derived if the ionized mass, hydrogen recombination flux and angular diameter are all known. Shklovsky (1956) first made the assumption of a constant ionized mass for all optically thin nebulae and, using published photographic magnitudes, derived distances to a large number of nebulae. Further important studies using this method were made by O'Dell (1962) and by Abell (1966), the former using photoelectric Hβ line fluxes. The Shklovsky constant ionized mass method has a number of associated difficulties. First, an estimate for the mean nebular radius is required, which involves a decision as to which isophotal point to choose and how to allow for non-circular morphologies. Secondly, a mean filling factor must be adopted. This filling factor allows not only for large-scale effects, such as empty central holes, but also for gas clumping on scales too small to assess from direct images. Finally, the assumption of a constant ionized mass for optically thin nebulae needs to be validated and calibrated using a sufficiently large sample of PN at known distances. Webster (1969) made the first attempt to derive absolute Hβ fluxes and ionized masses for PN in the Magellanic Clouds. Her values were employed by Seaton (1968), who provided the calibration for the large galactic PN distance catalogue of Cahn & Kaler (1971). More recent attempts at deriving ionized nebular masses for Magellanic Cloud PN have been made by Wood, Bessel & Dopita (1986), and Wood (1987), who employed the techniques of speckle interferometry and high-speed imaging to estimate angular diameters, and by Barlow (1987) who showed that [O II] doublet ratio electron densities could be used in a very straightforward manner to derive nebular ionized masses.

Distances to PN which are optically thick in the Lyman continuum (ionization bounded) can be derived by assuming a constant Hβ flux, since if PN evolve from similar progenitor stars, they should have similar ionizing luminosities and hence similar Hβ fluxes during their optically thick phase. This optically thick distance method was first applied to PN by Zanstra (1931) and Vorontsov-Velyaminov (1934). Minkowski (1965) pointed out that, if both the constant ionized mass and constant Hβ flux methods are applied to establish the distance to a PN, the correct method is the one which gives the lower distance.

In this paper, we use the recent calibrations for Magellanic Cloud PN nebular masses and dereddened Hβ fluxes from Barlow (1987) and Barlow, Monk, Walton & Clegg (1992, in preparation, hereafter referred to as BMWC). The latter work presents ionized masses based on [O II] doublet ratios for 80 Magellanic Cloud PN. They plot the ionized hydrogen mass versus [O II] electron density to show that the transition from optically thick to optically thin nebulae occurs for non-Type I (or 'standard') PN† when the nebular electron density falls below 4500 cm^{-3}. The 35 non-Type I PN in their sample with $500 \lesssim n_e(\mathrm{O\ II}) \lesssim 4500$ cm^{-3} had a mean ionized hydrogen mass of $0.217 \pm 0.079 M_\odot$ (corresponding to a total ionized nebular mass of $0.31 \pm 0.11 M_\odot$). For this group of nebulae, the ionized mass exhibited no dependence on density, so the essential requirement of the Shklovsky method, namely that all optically thin PN have the same ionized mass, is satisfied for non-Type I PN with $500 \lesssim n_e(\mathrm{O\ II}) \lesssim 4500$ cm^{-3}. Since there was no difference between the mean ionized mass derived for Small Magellanic Cloud (SMC) and Large Magellanic Cloud (LMC) PN, for which the metallicity difference is as large as that between LMC and Milky Way PN, it seems reasonable to adopt the same ionized mass for optically thin galactic PN as found for SMC and LMC PN.

Using the Hβ fluxes measured for Magellanic Cloud PN by Meatheringham, Dopita & Morgan (1988) and Wood *et al.* (1987), along with reddening estimates, BMWC also found that 18 'standard' PN in the SMC and LMC with $n_e(\mathrm{O\ II}) > 5000$ cm^{-3} had a mean dereddened Hβ flux (in cgs units) equivalent to $\log I(\mathrm{H}\beta) = -8.98 \pm 0.11$ at 1 kpc.

Along with the constant Hβ flux method for optically thick PN, we use a variant of the Shklovsky constant ionized mass method for optically thin PN that was proposed by Barlow (1987), which requires knowledge only of the dereddened Hβ flux and the electron density given by the mean [O II] doublet ratio for the whole nebula. In particular, knowledge of a mean nebular angular diameter and filling factor are not required, significantly reducing the uncertainties in the derived distances (the method is recapitulated in more detail in Section 4).

Peimbert (1990) has cautioned against the use of these Magellanic Cloud calibrations for galactic PN. He implies that the optically thin method of Barlow (1987) assumes a filling factor of 0.65 in order to obtain the ionized mass calibration, whereas the method is in fact independent of assumptions of both filling factor and angular radius. A filling factor of 0.65 was used by Barlow (1987) purely for purposes of comparison with the classical Shklovsky method calibrations of O'Dell (1962) and Cahn & Kaler (1971), who both adopted that value (a mean filling factor of 0.40 can be derived for the optically thin PN in our current sample, see the Appendix). Peimbert also criticizes the method used here on the grounds that there is a selection effect in favour of PN with large Hβ fluxes, whereas in fact the dereddened Hβ fluxes of the PN in the samples of Barlow (1987) and BMWC cover a range of a factor of 20. The [O II] densities of the Magellanic Cloud PN in the samples of Barlow (1987) and BMWC extend from 3×10^4 cm^{-3} down to 500 cm^{-3}, the same range of densities as is encountered in this sample of galactic PN. At lower densities than this, 'standard' PN tend to have very high-excitation spectra, rendering the [O II] doublet very difficult to detect in any case.

Integrated [O II] doublet ratios for entire nebulae are easy to obtain for the barely resolved PN in the Magellanic Clouds but do not in general exist for well-resolved PN in

†Type I PN are defined as those having N/O > 0.5 by number. As discussed by Peimbert (1978), Type I PN appear to originate from more massive than average progenitor stars. Their nebulae also appear to be more massive than those of non-Type I PN (Barlow 1987). In our own Galaxy, a 'standard' PN corresponds to the dominant Type II and Type III PN described by Peimbert (1978). As well as excluding Type I PN and the rare 'Halo' PN (i.e. Type IV PN, by Peimbert's 1978 definition), the term 'standard' excludes low-excitation PN having $I(5007)/I(\mathrm{H}\beta) < 4$. The relatively cool central stars of such low-excitation PN are unlikely to have reached their plateau ionizing luminosities yet.

our own Galaxy, published ratios coming from either single-aperture or long-slit spectra. We therefore initiated a programme to acquire integrated nebular [O II] doublet ratios for extended PN by obtaining long-slit spectra trailed at a uniform rate across the whole nebula during the exposure.

2 OBSERVATIONS AND DATA ANALYSIS

2.1 Observations

40 objects were observed using the 1-m Jacobus Kapteyn Telescope (JKT) at La Palma Observatory during 1989 December and 1990 August. A 2400 g mm^{-1} grating was used in the Richardson–Brealey spectrograph with a UV-coated GEC CCD as detector. The slit width was 1.5 arcsec, yielding a resolution of ~0.7 Å, as judged from the FWHM of comparison arc lines. The slit length was 6 arcmin. On-chip binning of 4 pixels perpendicular to the dispersion direction was performed upon readout. As we were only interested in high signal-to-noise ratio integrated fluxes, loss of spatial information was of no consequence. In order to obtain integrated spectra for extended nebulae, the slit was evenly scanned across the nebula during the exposure, thereby giving equal weight to all regions. Nebulae less than 2 arcsec in diameter were not scanned, as the seeing effectively 'trailed' the nebula.

The northern hemisphere sample was supplemented by long-slit spectra of 31 PN obtained at the 3.9-m Anglo–Australian Telescope (AAT). The spectra were obtained during runs in 1979 July, 1980 July, 1981 July, 1986 November, 1987 December and 1988 June, all using the RGO Spectrograph 25-cm camera with the IPCS as detector. A 1200 g mm^{-1} grating was used in first and second order, giving spectral dispersions of 33 and 10 Å mm^{-1} and corresponding resolutions of 1.3 and 0.4 Å. None of these nebulae was scanned spatially. Finally, IC 4997 and NGC 2371-2 were observed in 1988 October with the 2.5-m Isaac Newton Telescope (INT) at the La Palma Observatory, using the Intermediate Dispersion Spectrograph 235-mm camera with a 1200 g mm^{-1} grating in first order, with the IPCS as detector.

Table 1 presents a journal of the observations listing the object discovery name (in Right Ascension order), the PK number, the date of observation, the telescope used, the spectral resolution, the exposure time and the slit width in arcseconds. The nebular angular diameters are also presented, along with references for these diameters.

2.2 Data analysis

The JKT data were reduced using the FIGARO package (Shortridge 1989) at the University College London STARLINK node. The spectral images were initially bias-subtracted, divided by a normalized flat-field and cleaned of cosmic rays. The spectra were then extracted and wavelength calibrated with respect to a Cu–Ar comparison arc spectrum. The final spectra were not flux calibrated, as we were only interested in the flux ratio of the adjacent λλ3726, 3729 lines. Some of the JKT data (primarily from the 1990 August run) suffer from a pedestal effect due to imperfect charge transfer of the CCD upon readout (no pre-flash had been recommended). This caused an accumulation of charge blueward of each line, with a consequent smearing out of the line profile. A pedestal of fixed height (for a given spectrum) was present shortward of each line in some spectra. This effect caused a problem with the [O II] doublet in that λ3726 was contaminated by a component of λ3729. Although the flux was smeared out, the total flux in each line could be deconvolved by multiple Gaussian fitting (see next section). Very strong sources and very weak sources were not affected by this problem.

Some configurations of the AAT RGO Spectrograph 25-cm camera + IPCS produced a 'ghosting' effect in the spectral lines (usually when the [O II] lines fell near the detector edge). Data obtained in 1986 November and 1988 June (16 objects, although three were reobserved at other times) suffered from this problem; each emission line has a weak secondary component displaced to the red with an intensity of about 5–8 per cent of the main component (see below). Thus the flux in [O II] 3729 Å was slightly contaminated by the ghost of 3726 Å. This problem was also corrected by performing a four-Gaussian fit to each [O II] doublet. For the 1987 December and 1979 July spectra, the spectrograph configuration was such that the [O II] doublet was centred in the detector coverage and no 'ghosting' was present in these spectra.

The flux ratio of 3726–3729 Å was measured with the STARLINK DIPSO package (Howarth & Murray 1988), using the emission-line fitting routine ELF, written by P. J. Storey. This program performs a least-squares fit of Gaussian line profiles to spectral lines and can allow for either constrained or unconstrained central wavelengths, FWHM and peak intensities for each line. To fit the [O II] doublets, the program was allowed to find the central wavelength of λ3726 and its FWHM. The wavelength separation to λ3729 was set equal to the theoretical separation of the doublet, 2.78 Å, and the FWHM of λ3729 was constrained to be the same as for λ3726. The errors on the flux in each line take the variation in continuum level into account and are propagated in quadrature (subtracting the cross-term) to obtain the error on the flux ratio.

In the case of the JKT data where the poor charge transfer pedestal effect was occasionally present, the doublets were fitted by four Gaussians; one for each primary component and one for each pedestal. The intensity and FWHM of the pedestal and the wavelength separation of the pedestal from the main line were determined by fitting double-Gaussian profiles to H9 3835 Å and/or H10 3798 Å. These parameters were then adopted for Gaussian fits to the pedestals in the [O II] lines. On average, the FWHM of the pedestal was 1.7 Å and its mean wavelength separation was −0.9 Å from the main line. In the case of the AAT spectra where 'ghosting' occurred, four-Gaussian fitting was also used, but with a slightly different approach. The ghosts were assumed to have a fixed intensity ratio and wavelength separation with respect to the parent lines. Their parameters were derived by two-Gaussian fits to unblended emission lines in the spectra (generally [Ne III] 3868 Å). In the 1986 November spectra the 'ghosts', with 8 per cent of the parent line flux, were displaced by +1.60 Å, while in the 1988 June run, the 'ghosts' contained 5 per cent of the flux in the parent line and were displaced by 1.44 Å to the red.

Table 2 presents the [O II] flux ratio derived from each observation, together with the estimated error on the ratio.

Table 1. Run details.

	Object	PK	Date	Telescope	Resln. (Å)	Exp. Time (sec)	Slit Width (arcsec)	Diameter (arcsec)	Ref.[1] (Diam)
*	NGC 40	120+09.1	Dec. 89	JKT	0.7	1627	1.5	48.6	CSPTP83
*	Hu 1-1	119–06.1	Dec. 89	JKT	0.7	1506	1.5	10	ZPB89
*	BB 1	108–76.1	Dec. 87	AAT	1.5	300	1.3	–	
*	IC 351	159–15.1	Aug. 90	JKT	0.7	1987	1.5	7	AK90
*	IC 2003	161–14.1	Aug. 90	JKT	0.7	1865	1.5	10.5	CJA87
*	K 3-67	165–09.1	Dec. 89	JKT	0.7	1800	1.5	2.2	AK90
*	IC 418	215–24.1	Dec. 89	JKT	0.7	500	1.5	12.4	M81
			Dec. 87	AAT	1.5	100	1.3		
*	M 1-5	184–02.1	Dec. 89	JKT	0.7	1500	1.5	2.3	AK90
	IC 2149	166+10.1	Dec. 89	JKT	0.7	1500	1.5	12.2	CJA87
*	IC 2165	221–12.1	Dec. 89	JKT	0.7	1664	1.5	10	CJA87
*	J 900	194+02.1	Dec. 89	JKT	0.7	1789	1.5	6.0	AK90
	M 1-8	210+01.1	Nov. 86	AAT	1.5	700	1.0	18.4	PK67
	M 3-1	242–11.1	Nov. 86	AAT	1.5	250	1.0	11	ZPB89
*	M 1-11	232–04.1	Dec. 89	JKT	0.7	1500	1.5	2.2	AK90
			Dec. 87	AAT	1.5	300	0.7		
*	M 1-12	235–03.1	Dec. 87	AAT	1.5	200	1.0	1.8	AK90
	M 1-13	232–01.1	Dec. 87	AAT	1.5	250	1.7	15	A73
	NGC 2371-2	189+19.1	Oct. 88	INT	1.5	133	1.5	57.2	CJA87
	M 3-3	221+05.1	Dec. 87	AAT	1.5	210	1.3	12.3	PK67
			Nov. 86	AAT	1.5	300	1.0		
*	NGC 2392	197+17.1	Dec. 89	JKT	0.7	1898	1.5	36	CJA87
	NGC 2452	243–01.1	Dec. 87	AAT	1.5	105	1.3	18.8	PK67
	M 3-6	254+05.1	Dec. 87	AAT	1.5	80	1.5	11	ZPB89
*	NGC 3242	261+32.1	Dec. 89	JKT	0.7	1969	1.5	44	CJA87
*	IC 3568	123+34.1	Dec. 89	JKT	0.7	3375	1.5	13.6	CJA87
	H 4-1	049+88.1	Jun. 88	AAT	1.5	70	1.0	2.7	KM81
	NGC 5189	307–03.1	Jul. 79	AAT	0.32	300	0.9	140	PK67
			Jul. 79	AAT	1.0	100	1.5		
	He 2-97	307–09.1	Jul. 79	AAT	0.32	335	0.9	<3	MA82
(*)	NGC 5307	312+10.1	Jul. 79	AAT	0.32	500	0.9	13	M81
			Jul. 79	AAT	1.0	60	1.5		
(*)	He 2-108	316+08.1	Jul. 79	AAT	0.32	300	0.9	11	A82
	He 2-111	315–00.1	Jun. 88	AAT	1.5	140	1.0	31.4	PK67
	He 2-112	319+06.1	Jun. 88	AAT	1.5	60	1.0	14.6	MA75
(*)	He 2-113	321+03.1	Jul. 79	AAT	0.32	450	0.9		
(*)	NGC 5873	331+16.1	Jul. 79	AAT	0.32	250	0.9	7	M81
			Jul. 79	AAT	1.0	30	1.5		
(*)	NGC 5882	327+10.1	Jul. 79	AAT	0.32	300	0.9	14.3	M81
*	Me 2–1	342+27.1	Aug. 90	JKT	0.7	2000	1.5	7	AK90
(*)	He 2-138	320–09.1	Jul. 79	AAT	0.32	1000	0.9	7	MA75
*	IC 4593	025+40.1	Aug. 90	JKT	0.7	949	1.5	13	CJA87
*	Sn 1	013+32.1	Aug. 90	JKT	0.7	1800	1.5	3:	AK90
*	NGC 6210	043+37.1	Aug. 90	JKT	0.7	1185	1.5	13	PK67
*	H 2-1	350+04.1	Jul. 79	AAT	0.34	210	0.9	2.2	ZPB89

Table 1 – *continued*

	Object	PK	Date	Telescope	Resln. (Å)	Exp. Time (sec)	Slit Width (arcsec)	Diameter (arcsec)	Ref.[1] (Diam)
	IC 4642	334–09.1	Jun. 88	AAT	1.5	450	1.0	16.4	CJA87
*	NGC 6445	008+03.1	Aug. 90	JKT	0.7	2200	1.5	36	JDK86
*	NGC 6543	096+29.1	Aug. 90	JKT	0.7	1939	1.5	23.4	JDK86
*	NGC 6565	003–04.5	Aug. 90	JKT	0.7	1838	1.5	10	CJA87
*	NGC 6572	034+11.1	Aug. 90	JKT	0.7	1299	1.5	14	JDK86
*	NGC 6644	008–07.2	Aug. 90	JKT	0.7	1800	1.5	2.5	PK67
	NGC 6751	029–05.1	Nov. 86	AAT	1.5	400	1.0	20	CJA87
*	IC 4846	027–09.1	Aug. 90	JKT	0.7	2100	1.5	2.9	AK90
*	Vy 2-2	045–02.1	Nov. 86	AAT	1.5	670	1.2	0.4	SD83
	He 2-436	004–22.1	Nov. 86	AAT	1.5	350	1.2	< 10	PK67
*	NGC 6803	046–04.1	Aug. 90	JKT	0.7	1915	1.5	5.5	CJA87
*	NGC 6807	042–06.1	Aug. 90	JKT	0.7	1800	1.5	0.8	AK90
*	BD+30°3639	064+05.1	Aug. 90	JKT	0.7	1346	1.5	13	CJA87
*	NGC 6818	025–17.1	Aug. 90	JKT	0.7	1902	1.5	22	CJA87
*	NGC 6833	082+11.1	Aug. 90	JKT	0.7	1330	1.5	0.5	AK90
*	NGC 6886	060–07.2	Aug. 90	JKT	0.7	1685	1.5	5	CJA87
*	NGC 6891	054–12.1	Aug. 90	JKT	0.7	1960	1.5	11	CJA87
*	IC 4997	058–10.1	Aug. 90	JKT	0.7	1877	1.5	1.6	KM81
			Nov. 86	AAT	1.5	30	1.2		
			Oct. 88	INT	1.5	20	1.5		
*	NGC 7009	037–34.1	Aug. 90	JKT	0.7	1383	1.5	29.3	CJA87
			Jul. 79	AAT	0.34	1500	0.9		
*	NGC 7026	089+00.1	Dec. 89	JKT	0.7	1852	1.5	22.6	CJA87
*	NGC 7027	084–03.1	Aug. 90	JKT	0.7	1800	1.5	14.1	CJA87
*	K 648	065–27.1	Nov. 86	AAT	1.5	180	1.2	–	
*	IC 5117	089–05.1	Dec. 89	JKT	0.7	1800	1.5	1.5	AK90
*	Hu 1-2	086–08.1	Aug. 90	JKT	0.7	1820	1.5	8.4	A73
	IC 5148-50	002–52.1	Nov. 86	AAT	1.5	350	1.0	135	CJA87
*	Me 2-2	100–08.1	Dec. 89	JKT	0.7	1500	1.5	1.2	AK90
*	NGC 7662	106–17.1	Aug. 90	JKT	0.7	1914	1.5	33	CJA87
*	Hb 12	111–02.1	Dec. 89	JKT	0.7	1500	1.5	0.7	AK90

Notes: * indicates that the measured [O II] doublet ratio is an integrated value; (*) indicates that the adopted [O II] doublet ratio is a weighted mean (see text); [1]references follow Table 5.

2.3 Long-slit spectra

The long-slit AAT and INT spectra only sampled a strip through each nebula and consequently do not provide an integrated flux measurement of the [O II] doublet ratio. Tables 3 and 4 present the [O II] doublet ratio as a function of position in arcseconds across the nebula for these long-slit spectra. The position angle is given, along with the dispersion. Each spatial increment along the slit was 2.2 arcsec in length for the AAT spectra and 1.5 arcsec in length for the INT spectra (the slit widths used are listed in Table 1). For these objects, instead of adopting a straight mean of all the [O II] doublet ratios along the slit, a 'circular' integral was estimated to approximate the [O II] doublet ratio appropriate for the entire nebula. To do this, the spectrum in each spatial increment was assumed to represent the mean spectrum of a semi-annulus of thickness 2.2 arcsec, having a radius equal to the distance of the centre of the spatial increment from the central star. The flux from each doublet component in each spatial increment was therefore weighted by the area of its corresponding semi-annulus in order to obtain an overall weighted [O II] doublet ratio for the entire nebula. Although this may be a somewhat crude approximation, it is probably better than taking an average along the slit. The nebulae to

Table 2. [O II] doublet ratios.

Object	F(3726)/F(3729)	notes	log(n_e)	n_e(OII) (cm^{-3})	t(NII)	t(OIII)	Ref.[1] (t)	notes[2]
NGC 40	1.36±0.032		3.08±.02	1200^{+60}_{-50}	0.78	1.07	CPTP83	LE, WC 8[3]
Hu 1-1	1.32±0.051		3.12±.04	1320^{+110}_{-110}	1.02	1.15	AC83	
BB 1	1.76±0.070		3.52±.05	3310^{+400}_{-360}	1.06	1.42	BS	Halo
IC 351	1.96±0.68		3.65±.6	4470:	–	1.20	AC79	WR-Of[3]
IC 2003	2.45±0.25		4.11	13200:	1.32	1.20	KB	WC early
K 3-67	2.68±0.44		4.48:	30200:	1.35	1.35	AK87	Type I
IC 418	2.50±0.080	Dec. 89	4.12±.1	13200^{+4200}_{-2700}	0.83	0.91	TPP77	LE, Of(H)
	2.27±0.060[m]	Dec. 87						
M 1-5	2.47±0.53		4.09	12300:	1.05	0.91	Ba78	
IC 2149	1.90±0.052		3.57±.04	3720^{+330}_{-310}	0.88	1.00	TPP77	Of(H)
IC 2165	2.00±0.15		3.70±.12	5010^{+1300}_{-980}	0.83	1.39	TPP77	
J 900	1.91±0.11		3.60±.08	3980^{+790}_{-650}	1.06	1.18	AC83	
M 1-8	0.77±0.039[m]		2.18±.02	140±60	0.96	1.21	KB	(Type I)
M 3-1	1.24±0.040[m]		3.03±.04	1070^{+100}_{-90}	1.00	1.10	KB	
M 1-11	2.65±0.61	Dec. 89						
	2.47±0.13	Dec. 87	4.08±.17	1200^{+6600}_{-3500}	0.85	(0.95)	A83	VLE
M 1-12	2.48±0.066		4.10±.06	12600^{+1850}_{-1640}	0.91	(0.95)	A83	VLE
M 1-13	1.19±0.017[m]		2.95±.02	890^{+40}_{-40}	0.95	1.15	KB	Type I
NGC 2371-2	1.1±0.1[m]		2.91	810	0.98	1.33	PTP87	(Type I?), WC early
M 3-3	0.89±0.021[m]	Dec. 87	2.52±.05	330^{+40}_{-40}	0.99	1.26	KB	Type I
	0.91±0.031[m]	Nov. 86						
NGC 2392	1.35±0.050		3.19±.05	1550^{+170}_{-160}	1.20	1.46	Ba78	Of(H)
NGC 2452	1.27±0.077[m]		3.07±.07	1170^{+210}_{-170}	1.20	1.20	KB	Type I, WC 2
M 3-6	1.81±0.068[m]		3.48±.05	3020^{+370}_{-330}	–	0.95	KB	
NGC 3242	1.61±0.13		3.36±.07	2290^{+400}_{-340}	–	1.09	AC83	O(H)
IC 3568	1.59±0.43		3.33±.9	2140:	–	1.04	Ba78	O3(H)
H 4-1	1.06±0.029		2.84±.03	690^{+50}_{-50}	1.11	1.20	BS	Halo
NGC 5189	1.05±0.040[m]	33Å/mm	2.84	690	–	1.31	KB	Type I, WC 2
	1.04±0.020[m]	10Å/mm	2.82	660				
He 2-97	2.57±0.064[c]		4.23	17000	–	0.92	KB	
NGC 5307	1.61±0.11[c]	10Å/mm			–	1.20	KB	
	1.88±0.035[c]	33Å/mm	3.58	3800				
He 2-108	1.08±0.032[c]		2.80	630	(0.86)	0.98	A83	LE, Of(H)
He 2-111	1.11±0.024[m]		2.89±.02	780^{+30}_{-40}	1.10	1.91	KB	Type I
He 2-112	1.66±0.035		3.40±.02	2510^{+120}_{-110}	1.15	1.36	KB	Type I
He 2-113	2.15±0.15[c]		3.75	5690	(0.9)			VLE, WC 10
NGC 5873	2.35±0.094[c]	10Å/mm						
	2.07±0.052[c]	33Å/mm						
	2.14±0.05[c]	mean	3.81	6460	–	1.31	GMC83	
NGC 5882	2.01±0.060[c]		3.64	4370	0.83	0.92	TPP77	Of(H)
Me 2–1	1.45±0.14		3.26±.12	1820^{+540}_{-410}	1.16	1.31	AKC81	
He 2-138	2.05±0.051[c]		3.64	4370	0.79	–	A83	VLE, O(H)
IC 4593	1.49±0.070		3.22±.07	1660^{+340}_{-330}	1.14	0.91	Ba78	O5f(H)
Sn 1	1.34±0.28		3.11±.20	1290^{+750}_{-480}	–	1.02	Ba78	
NGC 6210	2.09±0.15		3.72±.2	5250^{+3070}_{-1940}	0.96	0.95	Ba78	O(H)

Table 2 – *continued*

	Object	F(3726)/F(3729)	notes	log(n_e)	n_e(OII) (cm^{-3})	t(NII)	t(OIII)	Ref.[1] (t)	notes[2]
	H 2-1	2.18±0.044[c]		3.80	6310	0.94	(0.96)	A83	VLE
	IC 4642	1.15±0.23[m]		2.99±.28	980^{+690}_{-530}	–	1.55	KB	
*	NGC 6445	1.18±0.092		3.00±.1	1000^{+300}_{-270}	–	1.30	Ka78	Type I
*	NGC 6543	1.98±0.027		3.59±.03	3890^{+490}_{-440}	0.96	0.82	AC83	Of-WR(H)
*	NGC 6565	1.68±0.051		3.41±.04	2570^{+250}_{-230}	0.95	1.03	AKF88	
*	NGC 6572	2.22±0.027		3.82±.04	6610^{+750}_{-680}	1.15	0.92	TPP77	Of-WR(H)
*	NGC 6644	2.05±0.058		3.73±.05	5370^{+1000}_{-800}	1.10	1.25	AKF88	
	NGC 6751	1.29±0.048[m]		3.02±.05	1050^{+120}_{-120}	0.81	0.96	KB	WC 4
*	IC 4846	2.90±0.29		high n_e lim		1.00	0.97	AC83	
*	Vy 2-2	2.36±0.20		4.02±.2	10500^{+5200}_{-3300}	–	1.40	SD83	
	He 2-436	2.78±0.22[m]		high n_e lim		–	1.02	M89	WR [4]
*	NGC 6803	2.98±0.30		high n_e lim		0.92	0.92	TPP77	
*	NGC 6807	2.97±0.30		high n_e lim		–	1.12	AK87	
*	BD+30°3639	2.60±0.059		4.27±.08	18600^{+3800}_{-3100}	0.82	–	TPP77	VLE, WC 9[3]
*	NGC 6818	1.57±0.064		3.35±.05	2240^{+260}_{-230}	1.14	1.26	AC79	
*	NGC 6833	3.95±1.22		high n_e lim		–	1.22	Ba78	
*	NGC 6886	2.08±0.079		3.76±.08	5750^{+1100}_{-900}	1.06	1.30	AC79	
*	NGC 6891	1.92±0.19		3.57±.15	3720^{+1160}_{-1080}	–	0.93	AK87	Of(H)
*	IC 4997	2.79±0.15	Aug. 90						
		2.44±0.098	Nov. 86						
		2.32±0.14[c]	Oct. 88						
		2.49±0.071	mean	4.91±.091	15500^{+3600}_{-2900}	–	1.50	BKN	Of[5]
*	NGC 7009	2.29±0.23	Aug. 90						
		1.96±0.078[c]							
		1.99±0.074	mean	3.64±.06	4350^{+660}_{-550}	1.00	1.00	KB	O(H)
*	NGC 7026	1.86±0.14		3.51±.13	3240^{+1180}_{-880}	0.98	0.91	AC79	WC 3
*	NGC 7027	2.45±0.063		4.12±.08	13300^{+2600}_{-2100}	1.35	1.35	M90	
*	K 648	1.74±0.15		3.48±.12	3020	1.06	1.25	A83	LE, in M15
*	IC 5117	2.61±0.67		4.34:	21900:	1.25	1.23	AC79	
*	Hu 1-2	2.39±0.24		4.05±.2	11200^{+6600}_{-4100}	1.34	1.85	PTP87	Type I
	IC 5148-50	0.79±0.15[m]		2.27±.09	190^{+40}_{-40}	(1.21)	1.45	KB	hgO(H)
*	Me 2-2	2.50±0.15		4.15±.2	14100^{+5200}_{-3700}	1.06	1.16	PTP87	Type I
*	NGC 7662	1.72±0.10		3.47±.09	2950^{+830}_{-600}	–	1.30	AC83	
*	Hb 12	2.05±0.10		3.69±.08	4900^{+990}_{-820}	0.98	1.25	AC83	LE

Notes: [m]adopted [O II] doublet ratio is a mean of all spatial increments and hence is not an integrated value; [c]adopted [O II] doublet ratio is weighted according to the 'circular integral' method (see text); [1]references follow Table 5; [2]PN central star types from Mendez (1991), except where otherwise noted; [3]Smith & Aller (1969); [4]M89; [5]BKN.

which this 'circular integration' method was applied were NGC 5307, NGC 5873, He 2-97, NGC 5882, H 2-1, He 2-108, He 2-113, He 2-138 and NGC 7009 from the 1979 July AAT run and IC 4997 from the 1988 October INT run. Quantities derived for objects which depend on this circular integration method are flagged in all tables. For two larger objects, NGC 2371-2 and NGC 5189, the long-slit spectra did not include the whole nebula. In these two cases, a flux-weighted slit-averaged mean [O II] doublet ratio is presented in Table 2, but no further quantities are derived.

3 ELECTRON DENSITIES

The flux ratio of the $^2D^0_{3/2}$–$^4S^0_{3/2}$ and $^2D^0_{5/2}$–$^4S^0_{3/2}$ transitions of O^+ at 3726.03 and 3728.81 Å is sensitive to the electron density, n_e, of the nebula between ~100 and 20000 cm^{-3}

Table 3. [O II] doublet ratios in 1979 July long-slit spectra.

Object	NGC 5189	NGC 5189	He 2-97	NGC 5307	NGC 5307	He 2-113	NGC 5873	NGC 5873	NGC 5882	H 2-1	NGC 7009
Dispersion (Å mm^{-1})	10	33	10	10	33	10	10	33	10	10	10
P.A. (°)	180	180	180	180	180	180	180	180	180	180	225
Dist. from CS (arcsec)											
+ 11.0	0.79±10%	0.80±21.3%			1.48±18.7%						1.54±3.39%
+ 8.8	1.21±4.96%	0.82±19.5%		1.62:	1.95±3.49%				1.0:		1.65±1.95%
+ 6.6	0.98±3.06%	1.18±11.9%		1.41±5.70%	2.06±2.57%				1.90±6.16%		2.06±1.01%
+ 4.4	1.04±2.88%	0.85±3.53%		1.48±9.12%	1.97±2.86%		2.45±17.5%	2.75±11.9%	2.20±2.93%	1.7:	2.15±1.05%
+ 2.2	1.05±1.91%	1.12±1.79%	2.77±3.91%	–	1.43:	2.15±10.9%	2.37±3.93%	1.81±2.99%	2.26±2.68%	2.08±2.72%	1.99±2.25%
0	1.10±1.81%	1.18±2.54%	2.97±2.44%	1.38±17.5%	1.72:	1.69±5.52%	2.51±3.53%	2.30±3.68%	1.78±3.46%	2.40±1.68%	1.96±5.24%
− 2.2	1.06±1.89%	1.01±0.99%	2.16±2.67%	1.22±7.85%	1.75±3.51%	2.40±11.2%	2.00±3.06%	1.95±3.97%	2.02±2.46%	2.15±3.60%	2.13±4.93%
− 4.4	1.19±7.56%	1.20±2.50%		1.85±5.07%	1.64±2.10%		2.15±6.49%	2.14±18.9%	2.16±3.05%	1.3:	2.08±2.29%
− 6.6	1.08±4.63%	1.21±1.65%		1.49±8.99%	1.76±2.85%				1.47±3.46%		2.11±1.40%
− 8.8	1.00±10.6%	1.06±1.89%			1.52±10.8%				1.5:		1.95±1.27%
− 11.0	0.98±19.4%	1.14±1.75%									
						1.73±3.20%					

Object	He 2-108	He 2-138
Dispersion (Å mm^{-1})	10	10
P.A. (°)	180	180
Dist. from CS (arcsec)		
+ 5.5	0.85±3.85%	1.58±7.82%
+ 3.3	1.25±2.05%	2.12±2.45%
+ 1.1	1.41±2.56%	2.19±1.88%
− 1.1	1.37±3.17%	2.31±2.45%
− 3.3	1.27±3.11%	1.76±2.70%
− 5.5	1.27±2.58%	
− 7.7	1.09±4.34%	

and is only weakly dependent on temperature (see e.g. Osterbrock 1989; the density domain traced most accurately by this ratio lies between 500 and 10 000 cm^{-3}). We used the program RATIO (written by I. D. Howarth and modified by S. Adams) to solve the equations of statistical equilibrium for the first five levels of O^+ using transition probabilities from Zeippen (1982), collision strengths from Pradhan (1976) and level energies from Mendoza (1983) to obtain n_e as a function of T_e for each [O II] doublet ratio. As discussed by Barlow (1987), for most optically thin nebulae the [O II] emission traces (by recombination) the distribution of O^{2+}, the dominant oxygen ion. For such nebulae the electron temperature derived from the [O III] 5007/4363 ratio is the most appropriate to use when solving for the [O II] electron density. In other nebulae, such as Type I PN, there is often very strong [O II] emission originating from near to an optically thick zone, in which case it may be more appropriate to use the electron temperature derived from the [N II] 6584/5755 ratio. We have used [N II] temperatures, when available, for the Type I nebulae and for the low-excitation nebulae. [O III] temperatures were used for all other nebulae. For some nebulae, we have used temperatures derived from the [O III] 5007/4363 and [N II] 6583/5755 ratios given by spectrophotometry obtained at the AAT (Kingsburgh & Barlow, in progress), while for the remaining nebulae we have adopted [O III] and [N II] temperatures found in the literature. The [N II] and [O III] electron temperatures (where $t = T_e/10\,000$ K), the reference for the temperatures and the electron densities derived from the [O II] doublet ratio are presented in Table 2. The errors quoted for the densities are based on the estimated errors associated with the flux ratios. Objects where the [O II] doublet ratio does not come from an integrated flux measurement are flagged. All other objects are either extended and were trailed during the observation or are compact objects of size comparable to the entrance slit; thus their derived densities should be a true mean for the whole nebula.

4 DISTANCES

4.1 Distances to optically thin and optically thick PN

The method of deriving distances to optically thin PN using n_e(O II) was proposed by Barlow (1987). In the middle stages of a PN's lifetime, the nebular mass ejected by the progenitor star becomes fully ionized. This mass (M_{ion}) can be expressed as

$$M_{ion} = (1+4y)m_p \int_0^\infty \epsilon n_H(r) 4\pi r^2 dr, \qquad (1)$$

where y is the He/H ratio by number, m_p is the mass of a hydrogen atom, ϵ is the fraction of nebula which contains ionized material (i.e. the filling factor), $n_H(r)$ is the number density of hydrogen atoms as a function of radius and $4\pi r^2 dr$ is a differential volume element. The emission from a

Table 4. [O II] doublet ratios in 1988 October long-slit spectra.

Object	IC 4997		NGC 2371-2
Dist. from CS (arcsec)		Dist. from CS (arcsec)	
+ 3.0	2.24±18.3%	+ 22.5	1.43::
+ 1.5	2.62±5.05%	+ 21.0	0.92±4.72%
0	2.52±3.49%	+ 19.5	1.00±2.97%
- 1.5	2.61±3.17%	+ 18.0	0.90±1.89%
- 3.0	2.18±4.00%	+ 16.5	0.97±2.26%
- 1.5	1.66±6.58%	+ 15.0	1.23±3.34%
		+ 13.5	1.50±6.66%
		+ 12.0	0.6::
		+ 10.5	1.1:
		+ 9.0	0.68±17.6%
		+ 7.5	0.8::
		⋮	⋮
		- 16.5	1.7::
		- 18.0	-
		- 19.5	1.45±20.0%
		- 21.0	hdl::
		- 22.5	1.60±20.0%
		- 24.0	1.81±18.7%
		- 25.6	1.33±5.58%
		- 27.0	1.21±4.88%
		- 28.5	0.91±6.49%

hydrogen recombination line traces the emission of ionized hydrogen:

$$I(\mathrm{H}\beta)=\frac{\alpha_{\mathrm{eff}}^{\mathrm{H}\beta}h\nu_{\beta}}{4\pi D^2}\int_0^{\infty}\epsilon n_{\mathrm{e}}(r)n_{\mathrm{p}}(r)4\pi r^2\,dr, \tag{2}$$

where $I(\mathrm{H}\beta)$ is the dereddened Hβ flux, $\alpha_{\mathrm{eff}}^{\mathrm{H}\beta}$ is the Case B partial recombination coefficient, h is Planck's constant, ν_{β} is the frequency of Hβ, D is the distance to the nebula and $n_{\mathrm{e}}(r)$ and $n_{\mathrm{p}}(r)$ are the electron and proton densities as a function of radius. $I(\mathrm{H}\beta)$ is related to the observed integrated Hβ flux, $F(\mathrm{H}\beta)$, by

$$\log I(\mathrm{H}\beta)=\log F(\mathrm{H}\beta)+c(\mathrm{H}\beta), \tag{3}$$

where $c(\mathrm{H}\beta)$ is the logarithmic extinction at the wavelength of Hβ.

Equation (2) can be used with (1) to give

$$M_{\mathrm{ion}}=(1+4y)m_{\mathrm{p}}\frac{I(\mathrm{H}\beta)4\pi D^2}{\alpha_{\mathrm{eff}}^{\mathrm{H}\beta}h\nu_{\beta}\langle n_{\mathrm{e}}\rangle}, \tag{4}$$

where

$$\langle n_{\mathrm{e}}\rangle=\frac{\int_0^{\infty}\epsilon n_{\mathrm{e}}(r)n_{\mathrm{H}}(r)r^2\,dr}{\int_0^{\infty}\epsilon n_{\mathrm{H}}(r)r^2\,dr}. \tag{5}$$

It was shown in detail by Barlow (1987; equations 4–12) that, in optically thin nebulae where either O^+ or O^{2+} is the dominant ionization stage of oxygen, $\langle n_{\mathrm{e}}\rangle$ defined by equation (5) is equal to n_{e}(O II) within 5 per cent for nebular densities in the range 1000–5000 cm^{-3}; thus n_{e}(O II) can be used in equation (4). Equation (4) can then be rearranged so that the distance to an optically thin PN can be expressed in terms of its ionized hydrogen mass [$M_{\mathrm{H}}=M_{\mathrm{ion}}/(1+4y)$]:

$$D_{\mathrm{thin}}(\mathrm{kpc})=1.11\times10^{-6}t^{-0.45}\sqrt{\frac{M_{\mathrm{H}}n_{\mathrm{e}}(\mathrm{O\ II})}{I(\mathrm{H}\beta)}}, \tag{6}$$

where M_{H} is in $M_{\odot}$, $t=T_{\mathrm{e}}/10^4$ K and the temperature dependence is introduced via $\alpha_{\mathrm{eff}}^{\mathrm{H}\beta}$ (Hummer & Storey 1987).

In the absence of [O II] electron densities, the usual expression for the distance to an optically thin PN involves M_{H}, t, n_{e}, the filling factor ϵ, the nebular angular diameter 2θ (in arcsec), the electron-to-hydrogen number ratio γ, and $I(\mathrm{H}\beta)$, e.g.,

$$D_{\mathrm{thin}}(\mathrm{kpc})=0.160t^{-0.18}\left[\frac{\gamma M_{\mathrm{H}}^2}{\epsilon\theta^3 I(\mathrm{H}\beta)}\right]^{1/5}. \tag{7}$$

The use of equation (6) eliminates the need to guess the filling factor ϵ (which in fact can be derived once the distance has been established – see the Appendix). In addition, the need to estimate a mean angular diameter (dependent on the nebular morphology) is eliminated, provided that n_{e}(O II) is derived from an integrated flux measurement.

The distance to an optically thick PN may be derived using the assumption of a constant Hβ flux. During the initial optically thick phase of a PN's expansion, the central star luminosity changes only slowly as it evolves to higher effective temperatures and Schoenberner (1981) has shown that the number of ionizing photons emitted remains approximately constant. Since recombinations balance ionizations during the nebular optically thick stage, the photon flux in a hydrogen recombination line directly counts the number of ionizing photons and should be constant until the nebula becomes optically thin. During the optically thick phase, therefore, the dereddened Hβ flux, $I(\mathrm{H}\beta)$, should be inversely proportional to the square of the distance, so that

$$D_{\mathrm{thick}}(\mathrm{kpc})=\sqrt{\frac{I(\mathrm{H}\beta)_{1\ \mathrm{kpc}}}{I(\mathrm{H}\beta)}}. \tag{8}$$

4.2 Magellanic Cloud calibrations

As discussed in Section 1, Barlow (1987) and BMWC have found that the mean ionized hydrogen mass (M_{H}) of a sample of 15 SMC and 20 LMC non-Type I PN having $n_{\mathrm{e}}(\mathrm{O\ II})<4500$ cm^{-3} is $0.217\pm0.079\,M_{\odot}$, with no variation discernible for $500<n_{\mathrm{e}}(\mathrm{O\ II})<4500$ cm^{-3}. The density of 4500 cm^{-3} can be linked to PN evolution as the density at which a PN becomes optically thin to hydrogen ionizing photons for the first time. The transition density of ~4500 cm^{-3} has been independently confirmed by Meatheringham *et al.* (1988).‡ The standard deviation about the mean is

‡Dopita & Meatheringham (1991) have derived some Magellanic Cloud PN hydrogen masses significantly exceeding $0.22\,M_{\odot}$ but, as discussed by BMWC, these high masses can be attributed to too high extinctions having been derived from optical Balmer line ratios, when compared to the extinctions derived for the same objects from ultraviolet/optical He II line ratios.

small enough that an ionized hydrogen mass of $M_H = 0.217 M_\odot$ can be meaningfully used to derive Shklovsky distances to optically thin PN. For example, the application of this ionized hydrogen mass calibration to the 35 non-Type I Magellanic Cloud PN with $n_e(\mathrm{O\ II}) \lesssim 4500$ cm^{-3} in BMWC's sample (i.e. those PN which gave the calibration) would lead to a mean distance error of ± 21 per cent (using equation 6).

Thus, inserting $M_H = 0.217 M_\odot$ into equation (6), the distance to an optically thin 'standard' PN is given by

$$D_{\mathrm{thin}}(\mathrm{kpc}) = 5.17 \times 10^{-7} t^{-0.45} \sqrt{\frac{n_e(\mathrm{O\ II})}{I(\mathrm{H}\beta)}}. \quad (9)$$

For PN having $n_e > 4500$ cm^{-3} (i.e. the optically thick nebulae), BMWC found for 13 LMC and five SMC 'standard' PN that $\log I(\mathrm{H}\beta) = -8.98 \pm 0.11$ (cgs) at 1 kpc. The distance moduli adopted for the LMC and SMC were 18.35 and 18.8 mag respectively. The application of this calibration to the 18 optically thick Magellanic Cloud PN which gave the calibration would lead to a mean distance error of only ± 14 per cent. We adopt this Hβ calibration for optically thick galactic 'standard' PN, giving

$$D_{\mathrm{thick}}(\mathrm{kpc}) = \frac{3.24 \times 10^{-5}}{\sqrt{I(\mathrm{H}\beta)}}. \quad (10)$$

As discussed in the Introduction, the cool central stars of low-excitation PN are unlikely to have attained their plateau ionizing luminosities and so the Hβ fluxes from such nebulae are expected to be lower than those from 'standard' PN. For three SMC and three LMC low-excitation (LE) objects [those having $1 < I(5007)/I(\mathrm{H}\beta) < 4$], BWMC found that $\log I(\mathrm{H}\beta) = -9.08 \pm 0.10$ (cgs) at 1 kpc. This calibration yields

$$D_{\mathrm{thick}}(\mathrm{LE}) = \frac{2.88 \times 10^{-5}}{\sqrt{I(\mathrm{H}\beta)}}\ \mathrm{kpc}. \quad (11)$$

Type I PN have an optically thin calibration different from that for 'standard' PN. BMWC found that three SMC Type I PN having $n_e < 4500$ cm^{-3} yielded $M_H = 0.28 \pm 0.06 M_\odot$, while seven similar Type I PN in the LMC had $M_H = 0.36 \pm 0.09\ M_\odot$. Although the masses agree within the formal errors, as the LMC calibration covers a larger sample, it is employed for the galactic Type I PN in our sample with due caution, giving

$$D_{\mathrm{thin}}(\mathrm{Type\ I}) = 6.66 \times 10^{-7} t^{-0.45} \sqrt{\frac{n_e(\mathrm{O\ II})}{I(\mathrm{H}\beta)}}\ \mathrm{kpc}. \quad (12)$$

Only two Type I LMC PN in the sample of BMWC had $n_e > 4500$ cm^{-3} and therefore an optically thick calibration does not exist for them. For completeness, we list optically thick distances for galactic Type I PN based on the 'standard' PN calibration, but such distances must be considered highly unreliable.

4.3 Adopted quantities

The expressions derived in Section 4.2 require the adoption of a dereddened integrated Hβ flux for each nebula. Whilst reliable *observed* Hβ fluxes exist for many nebulae, estimates for the extinction parameter $c(\mathrm{H}\beta)$ are often less reliable, particularly if based on measured Balmer line decrements. Such decrements are often obtained from narrow-slit spectra and the narrow wavelength baseline upon which Balmer line extinction estimates are based further reduces their reliability. For high-excitation PN, extinction estimates based upon the ratio of fluxes of He II $\lambda\lambda$1640 and 4686 are better, due to the much longer wavelength baseline, but integrated $\lambda\lambda$1640 and 4686 fluxes exist for relatively few galactic PN. Extinction estimates based upon the ratio of Hβ and radio free–free fluxes can in principle give the most reliable extinction estimates, due to the very long wavelength baseline and the availability of reliable integrated fluxes. Since the adoption of extinctions based on this method is equivalent to basing the technique on the radio fluxes alone, we transform, below, some of the expressions given in Section 4.2 into ones that make use of the measured radio flux from a PN, rather than its dereddened Hβ flux.

The ratio of free–free radio flux to Hβ flux can be expressed as a function of electron temperature and helium-to-hydrogen ratio (e.g. Milne & Aller 1975):

$$I(\mathrm{H}\beta) = \frac{3.28 \times 10^{-9} S_\nu(5\,\mathrm{GHz})}{t^{0.40} \ln(9900 t^{1.5})(1 + y^+ + 3.7 y^{++})}, \quad (13)$$

where S_ν(5 GHz) is the free–free radio flux at 5 GHz in Jy, y^+ is $n(\mathrm{He}^+)/n(\mathrm{H}^+)$ and y^{++} is $n(\mathrm{He}^{++})/n(\mathrm{H}^+)$. This expression can be substituted into equations (6) and (8) to obtain

$$D_{\mathrm{thin}} = 9.03 \times 10^{-3} t^{-0.25} \times \sqrt{\frac{n_e(\mathrm{O\ II}) \ln(9900 t^{1.5})(1 + y^+ + 3.7 y^{++})}{S_\nu(5\ \mathrm{GHz})}}, \quad (14)$$

$$D_{\mathrm{thick}} = 0.565 t^{0.20} \sqrt{\frac{\ln(9900 t^{1.5})(1 + y^+ + 3.7 y^{++})}{S_\nu(5\ \mathrm{GHz})}}, \quad (15)$$

in order to derive distances to 'standard' PN. Equations (14) and (15) imply that $D_{\mathrm{thick}} = D_{\mathrm{thin}}$ when $n_e(\mathrm{O\ II}) = 3915 t^{0.9}$ cm^{-3}. For the 43 standard PN in Table 2, the average value for t(O III) is 1.13, so on average a standard PN should become optically thin when its mean [O II] electron density drops below 4400 cm^{-3}.

Similar expressions for optically thin Type I PN and optically thick LE PN can be derived by inserting (13) into (12) and (11), respectively. The temperatures used in conjunction with (14) and (15) were the t(O III)s given in column 7 of Table 2. The helium abundances were derived from our AAT spectrophotometry, where available. The $\mathrm{He}^+/\mathrm{H}^+$ ratios take into account the correction for collisional excitation from the 2^3S state, following Clegg (1987). For the remaining nebulae, if dereddened helium line fluxes were available in the literature, helium abundances were derived taking into account the collisional corrections. Objects taken from the surveys of Torres-Peimbert & Peimbert (1977), Barker (1978), Aller & Czyzak (1979), Peimbert & Torres-Peimbert (1987) and Webster (1988) had helium abundances rederived from their published line intensities. If only abundances were presented, then they were adopted. Since the derived distance is only very weakly dependent on the adopted helium abundance, the collisional correction has

a negligible effect on derived distances. The 5-GHz fluxes are primarily taken from the recent Very Large Array (VLA) surveys of Zijlstra, Pottasch & Bignell (1989) and Aaquist & Kwok (1990). These surveys included roughly half the objects in our sample. For the rest of the objects, radio fluxes were taken from a compilation of other literature sources. When more than one radio flux measurement was available for a PN, an error-weighted mean flux was calculated. Fluxes at frequencies other than 5 GHz were converted to their 5-GHz equivalent using a $\nu^{-0.13}$ dependence for the free–free Gaunt factor, then included in the weighted average. Obviously discrepant fluxes and fluxes measured with a beamsize less than the angular diameter of the nebula were not included. Table 5 presents the 5-GHz fluxes and their sources, the helium abundances and their sources, the observed Hβ fluxes (also derived from error-weighted means of literature sources) and, for completeness, c(Hβ). For most cases, c(Hβ) was derived using equations (13) and (3), i.e. via the radio–(Hβ) method. In the few cases where radio fluxes had not been measured, were unreliable, or where there was reason to suspect that the free–free emission was not optically thin at the measured wavelength(s), I(Hβ) was derived from (3) using a c(Hβ) derived from the Balmer decrement or the [O II] 2470/7325-Å ratio.

Table 5. Hβ fluxes, reddenings, helium abundances, radio fluxes.

Object	S_ν(5 GHz) (mJy)	Ref. (S(5GHz))	He^+/H^+	He^{++}/H^+	Ref. (He)	−log F(Hβ)	Ref. (F(Hβ))	c(Hβ)[1]
NGC 40	459.5	c	0.044	0.000	CPTP83	10.66	c	0.42 (CPTP83)
Hu 1-1	26	ZPB89	0.064	0.008	Ka78	11.65	c	0.57
BB 1	<0.3	ZPB89	0.080	0.023	BS	12.57	BS	0.01 (BS)
IC 351	27	AK90	0.064	0.031	Ka78	11.43	c	0.30
IC 2003	50	AK90	0.047	0.051	KB	11.21	c	0.32
K 3-67	42	AK90	0.121	0.000	TS87	–	–	0.89 (TS87)
IC 418	1919.2	c	0.072	0.000	TPP77	9.57	c	0.30
M 1-5	70	AK90	0.10	0.000	Ba78	12.05	c	1.43
IC 2149	227	c	0.099	0.000	SK89	10.54	c	0.41
IC 2165	211.1	c	0.068	0.037	SK89	10.93	c	0.65
J 900	100	AK90	0.070	0.036	SK85	11.28	c	0.71
M 1-8	21	c	0.077	0.046	KB	12.37	CSC83	1.10
M 3-1	24	ZPB89	0.105	0.000	KB	11.29	c	0.16
M 1-11	108	AK90	0.021	0.000	KB	11.75	c	1.34
M 1-12	41	AK90	0.025	0.000	A83	11.60	A82	0.77
M 1-13	14	c	0.130	0.016	KB	11.76	c	0.35
NGC 2371-2	26.6	c	0.003	0.104	KB	10.99	c	0.00
M 3-3	<1	ZPB89	0.083	0.031	KB	12.32	KB	0.44
NGC 2392	282.8	c	0.049	0.043	TPP77	10.39	c	0.22
NGC 2452	60.0	c	0.047	0.073	KB	11.52	c	0.69
M 3-6	75	ZPB89	0.088	0.002	KB	10.78	CSC83	0.18
NGC 3242	848.5	c	0.077	0.023	SK89	9.72	c	0.11
IC 3568	83.9	c	0.091	0.001	SK85	10.82	c	0.25
H 4-1	< 0.3	AK90	0.093	0.008	BS	12.54	BS	0.01 (BS)
NGC 5189	411.8	c	0.062	0.080	KB	10.52	VP85	0.49
He 2-97	23.6	c	0.097	0.000	KB	11.44	c	0.35
NGC 5307	92.3	c	0.058	0.048	KB	11.18	c	0.56
He 2-108	37.2	c	0.110	0.000	A83	11.48	c	0.56
He 2-111	70.2	c	0.091	0.126	KB	12.01	SK89	1.06
He 2-112	77.8	c	0.089	0.050	KB	12.15	P71	1.41
He 2-113	(183.8)	c	0.000	0.000	KB	11.82	c	1.66
NGC 5873	42.9	c	0.069	0.041	SK89	11.09	c	0.12
NGC 5882	353.4	c	0.113	0.003	SK89	10.37	c	0.44
Me 2–1	27.1	AK90	0.049	0.072	SK89	11.35	c	0.15

Table 5 – *continued*

Object	S_ν(5 GHz) (mJy)	Ref. (S(5GHz))	He^+/H^+	He^{++}/H^+	Ref. (He)	$-\log F(H\beta)$	Ref. (F(Hβ))	$c(H\beta)$[1]
He 2-138	86.3	c	0.014	0.000	A83	10.71	c	0.25
IC 4593	95.6	c	0.087	0.000	SK85	10.57	c	0.09
Sn 1	7:	AK90	0.082	0.001	Ba78	11.72	c	0.27 (Ba78)
NGC 6210	283.6	c	0.097	0.002	SK85	10.09	c	0.06
H 2-1	69.2	ZPB89	0.055	0.000	A83	11.45	c	0.83
IC 4642	47.0	c	0.006	0.104	SK89	11.60	c	0.57
NGC 6445	339.6	c	0.165	0.061	KA78	10.69	c	0.57
NGC 6543	810.4	c	0.11	0.000	M89	9.60	c	0.06
NGC 6565	36.8	c	0.100	0.010	SK89	11.24	c	0.29
NGC 6572	1213	Mas89b	0.109	0.000	AC79	9.80	c	0.41
NGC 6644	97.1	c	0.102	0.015	SK89	11.02	c	0.44
NGC 6751	56.4	c	0.111	0.000	KB	11.27	c	0.54
IC 4846	43	AK90	0.084	0.001	SK89	11.34	c	0.50
Vy 2-2	(253)	c	0.116	0.003	SK89	11.57	c	1.39
He 2-436	16.8	c	0.087	0.000	M89	11.90	KB	0.64
NGC 6803	95.2	c	0.124	0.003	SK89	11.18	c	0.68
NGC 6807	29	AK90	0.103	0.000	SK85	11.45	c	0.39
BD+30°3639	62	Mas89b	0.042	0.000	Ba78	10.04	M89	0.42
NGC 6818	309.6	c	0.050	0.043	SK85	10.49	c	0.39
NGC 6833	21	AK90	0.101	0.002	Ba78	11.26	c	0.23 (Ba78)
NGC 6886	110.6	c	0.112	0.039	Ka80	11.42	c	0.85
NGC 6891	119.3	c	0.112	0.000	Ka80	10.65	c	0.25
IC 4997	–		0.090	0.000	BKN	10.48	F80	0.39 (F80)
NGC 7009	652.4	c	0.107	0.015	KB	9.79	c	0.09
NGC 7026	251.4	c	0.093	0.010	SK85	10.92	c	0.84
NGC 7027	(6957.0)	c	0.062	0.042	M90	10.12	SK82	1.37
K 648	4.69	JKG91	0.086	0.000	ASHAW84	12.15	c	0.12
IC 5117	264	c	0.098	0.008	SK85	11.39	c	1.26
Hu 1–2	221	c	0.056	0.092	PTP87	11.21	c	0.81 (PTP87)
IC 5148-50	–		0.096	0.042	KB	11.5:	KSK90	0.38 (KB)
Me 2-2	44.9	AK90	0.150	0.000	PTP87	11.17	c	0.28
NGC 7662	631	ZPB89	0.048	0.038	M89	9.99	c	0.20
Hb 12	400	AK90	0.10	0.000	Ba78	10.99	c	1.05 (Ba78)

Notes: [1] $c(H\beta)$ for most objects is derived with the radio–Hβ method; objects where $c(H\beta)$ has been adopted by other means are followed by the appropriate reference. c Values adopted from compilation of literature sources. 5-GHz radio fluxes in parentheses are estimated from optically thin fluxes measured at higher frequencies.

References for Tables 1, 2 and 5:

A73: Allen 1973. A82: Acker *et al.* 1982. A83: Adams 1983. AC79: Aller & Czyzak 1979. AC83: Aller & Czyzak 1983. AK87: Aller & Keyes 1987. AK90: Aaquist & Kwok 1990. AKC81: Aller, Keyes & Czyzak 1981. AKF88: Aller, Keyes & Feibelman 1988. ASHAW84: Adams *et al.* 1984. Ba78: Barker 1978. BKN: Barlow, Kindl & Nussbaumer, unpublished. BS: Barlow & Seaton, unpublished. CJA87: Chu, Jacoby & Arendt 1987. CSC83: Carrasco, Serrano & Costero 1983. CSPTP83: Clegg *et al.* 1983. F80: Flower 1980. GMC85: Gutierrez-Moreno, Moreno & Cortes 1985. GPGG83: Gathier *et al.* 1983. JDK86: Jewitt, Danielson & Kupferman 1986. JKG91: Johnson, Kulkarni & Goss 1991. Ka78: Kaler 1978. Ka80: Kaler 1980. KB: Kingsburgh & Barlow, in preparation. KM81: Kohoutek & Martin 1981. KSK90: Kaler, Shaw & Kwitter 1990. M81: Martin 1981. M89: Middlemass 1989. M90: Middlemass 1990. Mas89b: Masson 1989b. MA75: Milne & Aller 1975. MA82: Milne & Aller 1982. P71: Perek 1971. PK67: Perek & Kohoutek 1967. PTP87: Peimbert & Torres-Peimbert 1987. SD83: Seaquist & Davis 1983. SK85: Shaw & Kaler 1985. SK89: Shaw & Kaler 1989. TPP77: Torres-Peimbert & Peimbert 1977. TS87: Tamura & Shaw 1987. VP85: Viadana & de Freitas Pacheco 1985. Web83: Webster 1983. Web88: Webster 1988. ZPB89: Zijlstra *et al.* 1989.

Equations (14) and (15) have been applied to all the 'standard' PN in our sample. As discussed by Minkowski (1965), for a given PN the correct method is the one which gives the lower distance. If a PN is optically thick in the Lyman continuum, its ionized mass will be lower than assumed in equations (6) and (14) and so $D_{\rm thin}$ will overestimate the distance. If a PN is optically thin, its Hβ luminosity will be lower than assumed in equations (8) and (15) and so $D_{\rm thick}$ will overestimate the distance.

Table 6 presents, for each 'standard' PN, the derived values of $D_{\rm thin}$ (column 3) and $D_{\rm thick}$ (column 4), followed by the final adopted distance $D_{\rm adopt}$, the smaller of $D_{\rm thin}$ and $D_{\rm thick}$. Values of $D_{\rm thin}$ and $D_{\rm thick}$ derived from [O II] spectra that did not encompass the entire nebula are given in parentheses in Tables 6, 7 and 8. As discussed in Section 4.2, Type I PN and low-excitation (LE) PN are distinguished from 'standard' PN for the purpose of distance determination. Table 7 presents the distances derived for the galactic Type I PN in our sample. The LMC Type I mass calibration has been used for $D_{\rm thin}$ (see equation 12), while the Hβ flux calibration for standard PN has been used for $D_{\rm thick}$ (for completeness; this thick calibration may well be inappropriate for Type I PN. Values of $D_{\rm adopt}$ resulting from $D_{\rm thick}$ are listed in parentheses in Table 7). For low-excitation PN, the optically thick calibration corresponding to equation (11) was used. It was assumed that optically thin LE PN have the same ionized mass as 'standard' PN. Distances were not derived to very low-excitation (VLE) PN, where VLE PN are defined as those having $I(5007)/I(\mathrm{H}\beta) < 1$, as no suitable calibration exists for them at present.

Table 6. Distances to 'standard' PN.

Object	n_e(O II) (cm^{-3})	D_{thin} (kpc)	D_{thick} (kpc)	D_{adopt} (kpc)	$D_{literature}$ (kpc)
Hu 1-1	1320	6.30	11.56	6.30	
IC 351	4470:	11.71	11.92	11.7	7.68^{C}
IC 2003	13200:	15.14	8.97	8.97	
M 1-5	12300:	12.24	6.62	6.62	
IC 2149	(3790)	(3.71)	3.77	(3.71)	
IC 2165	5010	4.37	4.49	4.37	
J 900	3980	5.82	6.23	5.82	$\geq 4.2^{G}$
M 1-8	(140:)	(2.41)	13.93	(2.41)	
M 3-1	(1070)	(5.98)	11.95	(5.98)	
NGC 2392	1450	2.02	3.94	2.02	1.98^{C}, 2.7^{Me}
M 3-6	(3020)	(5.80)	6.46	(5.80)	
NGC 3242	2290	1.51	2.06	1.51	1.70^{C}, 2.0^{Me}
IC 3568	2140:	4.54	6.26	4.54	3.76^{C}, 3.5^{Me}
He 2-97	(17000)	(24.70)	11.41	11.4	
NGC 5307	(3800)	(5.98)	6.60	(5.98)	
NGC 5873	(6460)	(11.19)	9.86	9.86	
NGC 5882	(4370)	(3.28)	2.99	2.99	
Me 2-1	1820	7.76	12.88	7.76	
IC 4593	1660	3.82	5.63	3.82	4.30^{C}, 3.7^{Me}
Sn 1[a]	1290:	9.77	17.18	9.77	
NGC 6210	5250	3.95	3.33	3.33	1.66^{C}
IC 4642	(980)	(4.31)	10.53	(4.31)	
NGC 6543	3890	2.07	1.90	1.90	1.11^{C}, 3.0^{Me}
NGC 6565	2570	7.68	9.61	7.68	
NGC 6572	6610	2.16	1.60	1.60	0.90^{C}, 3.5^{Me}, $\leq 2.1^{G}$
NGC 6644	5370	6.66	6.30	6.30	3.95^{C}
NGC 6751	(1050)	(3.97)	7.52	(3.97)	2.98^{C}
IC 4846	hdl	–	8.55	8.55	4.91^{C}
Vy 2-2	10500	5.58	3.97	3.97	
He 2-436	(hdl)	–	13.86	13.9	
NGC 6803	hdl	–	5.78	5.78	$\geq 3.2^{G}$
NGC 6807	hdl	–	10.91	10.9	4.80^{C}
NGC 6818	2240	2.46	3.61	2.46	1.95^{C}
NGC 6833[a]	hdl	–	10.59	10.6	5.51^{C}
NGC 6886	5750	6.68	6.22	6.22	$\geq 1.5^{G}$
NGC 6891	3720	5.17	5.13	5.13	4.86^{C}, 3.8^{Me}
IC 4997[a]	15500	5.93	3.59	3.59	3.10^{C}, $\geq 1.3^{G}$
NGC 7009	4350	2.41	2.29	2.29	1.89^{C}, 2.4^{Me}
NGC 7026	3240	3.36	3.54	3.36	2.0^{C}, $\geq 2.5^{G}$
NGC 7027	13300	1.25	0.78	0.78	0.51^{C}, 0.88^{Ma}
IC 5117	21900:	9.92	3.75	3.75	2.88^{C}, $3.0:^{G}$
NGC 7662	2950	1.95	2.53	1.95	1.54^{C}

4.4 Sources of error

Few previous measurements have been made of integrated [O II] doublet ratios for entire PN. Lutz (1974) presented

Table 7. Distances to Type I PN.

Object	n_e(O II) (cm^{-3})	D_{thin} (kpc)	D_{thick} (kpc)	D_{adopt} (kpc)
K 3-67	30200:	29.98	9.63	(9.63)
M 1-13	(890)	(9.45)	16.43	(9.45)
M 3-3	(330)	(1.87)	5.57	(1.87)
NGC 2452	(1170)	(5.47)	8.45	(5.47)
He 2-111	(780)	(4.13)	9.66	(4.13)
He 2-112	(2510)	(6.76)	7.56	(6.76)
NGC 6445	1000	2.15	3.73	2.15
Hu 1-2[a]	11200	6.51	5.11	(5.11)
Me 2-2[a]	14100	20.60	9.03	(9.03)

Table 8. Distances to LE PN.

Object	n_e(O II) (cm^{-3})	D_{thin} (kpc)	D_{thick} (kpc)	D_{adopt} (kpc)	$D_{literature}$ (kpc)
NGC 40[a]	1200	2.29	4.27	2.29	1.78^{C}
IC 418	13200	2.39	1.25	1.25	0.76^{C}, 2.0^{Me}
He 2-108	(630)	(3.77)	9.31	(3.77)	
Hb 12[a]	4900	3.05	3.03	3.03	

Notes to Tables 6, 7 and 8.
[a]Indicates that the 5-GHz flux was unreliable or the object is optically thick in the free–free continuum, hence $I(\mathrm{H}\beta)$ was derived via equation (3), then used in equations (6) and (8) to derive $D_{\rm thin}$ and $D_{\rm thick}$. Quantities in parentheses have either been derived from an n_e(O II) which does not represent an integrated value [i.e. the adopted n_e(O II) is a straight or weighted mean of spatial increments which do not encompass the entire nebula] or via an uncertain calibration. $D_{\rm literature}$ references: ^{C} – Cudworth (1974); ^{Me} – Mendez *et al.* (1988, 1990); ^{Ma} – Masson (1989a); ^{G} – Gathier *et al.* (1986a).

integrated ratios, derived from photographic spectra, for 12 PN. For the seven PN in common with the current paper, the doublet ratios all agree within the quoted errors.

Apart from the nominal distance uncertainties of ±21 and ±14 per cent associated with the optically thin and thick methods (arising from the scatter in the ionized masses and absolute Hβ fluxes, respectively, of the Magellanic Cloud calibrators), distance errors could result if the Magellanic Cloud calibrations were applied to inappropriate galactic PN. The Magellanic Cloud PN used as calibrators include the brightest (i.e. the optically thick PN) but the overall Hβ luminosity range was a factor of 20 and sampled densities down to ~500 cm^{-3}. The galactic PN observed here sampled the same density range and thus selection effects are minimized. The uncertainty in the distance moduli of the LMC and SMC is usually estimated to be less than 0.3 mag, corresponding to a distance uncertainty of less than 15 per cent. Any error in the adopted Magellanic Cloud distances propagates linearly through to the distances derived for galactic PN.

Another question concerns the utility of [O II] as a nebular mass tracer. The older, lower surface brightness PN not treated here are generally of high excitation, so that the assumption that O^+ (produced by recombination of O^{2+}) traces a dominant ionization stage may no longer be valid. However, the extreme weakness of [O II] lines from such PN renders the [O II] method impracticable for them in any case. In general terms, [O II] provides the most suitable density-sensitive ratios for tracing nebular mass [see section 3 of Barlow (1987) for details]. The [O II] λλ3726, 3729 doublet is most useful as an ionized mass tracer within the range 900–6700 cm^{-3} (i.e. between the critical densities for the $^2D^0_{3/2,5/2}$ levels). At higher densities, the ratio of [O II] λλ3726+3729 to [O II] λ7325 is appropriate for tracing the mass (provided one obtains integrated fluxes), as the $^2P^0_{3/2,1/2}$ levels which give rise to λ7325 have a critical density of 5×10^6 cm^{-3}. The [Cl III] λλ5518, 5538 lines sample a similar but slightly more restricted ionization potential range than the [O II] lines, with critical densities of 7500 and 3.8×10^4 cm^{-3} for the respective upper levels. For a very highly ionized nebula, the [Ar IV] λλ4711, 4740 lines come from a more representative ionization stage than that sampled by the [O II] or [Cl III] transitions (the O^+ ions would arise from recombination of O^{2+}, which might not be the dominant ionization stage of oxygen in the nebula). However, the critical densities of the [Ar IV] λλ4711 and 4740 upper levels are 1.7×10^4 and 1.6×10^5 cm^{-3}, respectively. High-excitation PN normally have electron densities significantly lower than either of these values, so the [Ar IV] lines would not be useful mass tracers for them. For these and other nebulae, the ratio of the [O III] IR fine-structure lines $^3P_0$–$^3P_1$ at 88 μm and $^3P_1$–$^3P_2$ at 52 μm, with critical densities of 500 and 3600 cm^{-3} respectively, could provide a suitable mass tracer.

Another question associated with the distance methods used here concerns the applicability of the assumption that the nebulae are either completely optically thick or completely optically thin in the hydrogen Lyman continuum. A more realistic situation could be a PN which is thick in some directions, but thin in others (as in some bipolar nebulae). In this situation, both the optically thin and the optically thick distances would be overestimates. In a 'worst case' scenario, a PN could be 50 per cent thick and 50 per cent thin. Such a PN might have $I(H\beta)\sim\frac{3}{4}I(H\beta)_{1\,kpc}$ and an ionized mass $\sim M_H/2$. If the PN was at a distance of 1 kpc, the application of equations (15) and (14) would yield $D_{thick}=1.15$ kpc and $D_{thin}=1.40$ kpc. D_{thick} would be adopted and hence the distance would be overestimated by 15 per cent, a tolerable error. As the PN becomes increasingly optically thick or thin, the appropriate distance method quickly converges to the correct distance.

5 DISCUSSION OF INDIVIDUAL OBJECTS

5.1 Halo planetary nebulae

There are three halo planetary nebulae in our sample: K 648, which is a member of the globular cluster M15, BB 1 and H 4-1.

K 648 (=Ps 1=PK 65−27°1). We have used our measured [O II] electron density of 3020 cm^{-3}, the 5-GHz radio flux of 4.69 mJy measured by Johnson, Kulkarni & Goss (1991), the [O III] electron temperature of 12 500 K measured by Adams *et al.* (1984), and the known distance to M15 (9.7 kpc, Webbink 1985) in equations (6) and (13) to derive an ionized hydrogen mass of $M_H=0.042\,M_\odot$. At a density of 3020 cm^{-3} one would expect K 648 to be optically thin, and this assumption is confirmed by the distance of 25 kpc to K 648 given by the optically thick assumption (equation 11). The central star masses of halo PN, and therefore their plateau ionizing luminosities and optically thick Hβ fluxes, are not expected to be significantly smaller than those of standard PN. From a detailed analysis of the K 648 nebula and central star, Adams *et al.* (1984) concluded that the nebula was optically thin in the hydrogen Lyman continuum.

BB 1 (PK 108−76°1) and H 4-1 (PK 49+88°1). For these two galactic halo PN, we have adopted the same ionized hydrogen mass as found for K 648 in order to derive their optically thin distances. Comparison of the resulting D_{thin} with D_{thick} (Table 9) shows that both these halo PN are optically thin. As only upper limits to the radio fluxes from these two PN have been determined, we used the Hβ fluxes listed for them in Table 5, along with $c(H\beta)=0.01$ (Barlow & Seaton, in preparation), in equation (6).

5.2 Other PN

IC 4997 (PK 58−10°1), Vy 2-2 (PK 45−2°1) and Hb 12 (PK 111−2°1). These three PN are all examples of young, high-density ionized nebulae surrounded by neutral zones. H I

Table 9. Distances to halo PN.

Object	n_e(OII) (cm^{-3})	D^1_{thin} (kpc)	D_{thick} (kpc)	D_{adopt} (kpc)
K 648	3020	9.7[a]	25	9.7
BB 1	3310	29	62	29
H 4-1	690	10	60	10

Notes: [1]For $M_H=0.042\,M_\odot$; [a]adopted distance to M15 (Webbink 1985).

around IC 4997 has been detected in absorption at 21 cm (Altschuler *et al.* 1986), OH maser emission has been detected from the shell around Vy 2–2 (Seaquist & Davis 1983) and fluorescent H_2 emission has been detected from the shell around Hb 12 (Dinerstein, Carr & Harvey 1988). All three have a compact ionized core, with an angular diameter of 1.6 arcsec in the case of IC 4997 (Kohoutek & Martin 1981), 0.4 arcsec in the case of Vy 2–2 (Seaquist & Davis 1983), and 0.5 arcsec in the case of Hb 12 (Aaquist & Kwok 1991). The rms electron density derived for each of these cores is so high (see Tables A1 and A3 of the Appendix) that any [O II] emission ought to show a 3726/3729 ratio at the high-density limit of 2.875, whereas the observed ratios are all below this limit (see Table 2). The ratio of 2.05 ± 0.10 found for Hb 12 is the furthest from the high-density limit. Imaging of this PN by the VLA (see Bignell 1983; Aaquist & Kwok 1991) has revealed a faint V-shaped structure, of about 10-arcsec extent, with the dense core at its apex. The relatively low-density [O II] emission that we observe undoubtedly originates from this extended nebulosity. The material surrounding the dense core of Hb 12 must have a low enough optical depth in at least a few directions that ionizing photons can penetrate to lower density material. We hypothesize that the same situation also holds around the dense cores of Vy 2–2 and IC 4997. Indeed, the spatially resolved [O II] doublet ratio measurements obtained for IC 4997 (Table 4) show a decrease of the ratio on either side of the core.

NGC 7027 (PK 84−3°1). Our optically thick distance of 0.78 ± 0.11 kpc (Table 6) shows excellent agreement with the distance of 0.88 ± 0.15 kpc derived by Masson (1989a) from VLA proper motion measurements of the nebular expansion over a 4-year period. Since our optically thick calibration is based on the mean dereddened Hβ flux for 18 Magellanic Cloud PN, NGC 7027 does not therefore appear to be particularly overluminous compared to other optically thick PN.

Our integrated [O II] 3726/3729 ratio of 2.45 ± 0.06 is lower than the 1.2-arcsec slit photoelectric scanner value of 2.75 measured by Miller (1971) or the 4×2 arcsec^2 slot CCD echelle spectrum value of 2.70 measured by Aller & Keyes (1987). However, ratios between 2.00 and 2.38 had previously been reported for NGC 7027 and were interpreted by Seaton & Osterbrock (1957) as due to different slits intercepting different parts of the filamentary structure of this nebula.

IC 3568 (PK 123+34°1). Harrington & Fiebelman (1983) derived a constraint on M_H, ϵ and D (their equation 5: $M_H = 0.0117 \epsilon^{1/2} D^{5/2}$) based on a density distribution deconvolved from a VLA brightness distribution. From Table 6, we obtain $D = 4.54$ kpc (from the optically thin scale, which corresponds to $M_H = 0.217 M_\odot$), so the above relation implies $\epsilon = 0.18$.

6 COMPARISON WITH OTHER DISTANCE SCALES

The distance scale has been a source of longstanding debate in PN studies. In this section, we compare our distances with those obtained by previous investigators.

Previous applications of the classical Shklovsky method to galactic PN, using equation (7), have utilized optical angular radii and have assumed a mean filling factor ϵ between 0.6–0.7. Mallik & Peimbert (1988) found the PN in their study to show a great range in their derived ϵ, a finding that is confirmed here (see the Appendix). However, a large part of the range found in ϵ appears to be due to the difficulties in accurately defining the angular radius θ of a PN, since $\epsilon \propto \theta^{-3}$ (see equations A1 and A2 of the Appendix). A fit to the optically thin points plotted in Fig. A1 of the Appendix yields $\epsilon \propto (\theta D)^{-2.6}$, where D is the distance derived by the [O II] method, which we argue in the Appendix to be consistent with most of the spread in our derived filling factors being attributable to inaccuracies in the adopted angular radii (e.g. a change of 30 per cent in the adopted θ leads to a change of a factor of 2.2 in the derived ϵ). A mean filling factor of 0.40 ± 0.28 is derived for the optically thin PN that are plotted in Fig. A1 of the Appendix.

Equation (7) yields a relation of the form $D(\text{pc}) = K\theta^{-3/5} I^{-1/5}$, where θ is the nebular angular radius and I is the dereddened Hβ flux. For θ in arcsec and I in erg cm^{-2} s^{-1}, the present study implies $K = 106.6$ [we have $M_H = 0.217 M_\odot$, $\epsilon = 0.40$ (see Appendix); and the mean values of t(O III) and γ for the standard PN in Table 6 are 1.13 and 1.122, respectively].

O'Dell (1962) made the first quantitative application of the Shklovsky method to PN using photoelectrically measured Hβ fluxes. The nebular quantities adopted by O'Dell correspond to $K = 74.5$, giving a distance scale which is a factor of 1.43 smaller than the one derived here. For the 19 optically thin PN in Table 6 that are in common with the sample of O'Dell (1962), we find a mean distance ratio (us/O'Dell) of 1.61 ± 0.43. This ratio is consistent with the predicted one but may be slightly larger due to the adoption of differing extinctions. The adopted extinctions obtained from mean galactic relations are not listed by O'Dell.

O'Dell (1963) estimated a mean Hβ flux for optically thick galactic PN of $\log I(\text{H}\beta) = -9.0 \pm 0.1$. The Magellanic Cloud calibration for optically thick 'standard' PN (-8.98 ± 0.11; see Section 4.2) agrees extremely well with this.

Cahn & Kaler (1971; CK) adopted, from Seaton (1968), parameters for optically thin PN that yielded $K = 75.6$, very similar to the O'Dell (1962) scale. Their distance scale is therefore a factor of 1.41 smaller than ours. There are 11 optically thin standard PN in Table 6 that are in common with Cahn & Kaler's table 1 sample with individually determined extinctions. The mean distance ratio (us/CK) for this group is 1.55 ± 0.42, consistent with the predicted ratio [the extinctions derived by CK for this group are an average of 0.27 dex larger than those derived in Table 5, so by equation (7) this would give a further factor of 1.13 difference in distances, i.e. a total factor of $1.13 \times 1.41 = 1.60$]. As noted by Barlow (1987), the main Cahn & Kaler sample (their table 3) had extinctions derived from a galactic dust distribution model that overestimated $c(\text{H}\beta)$ by an average of 0.45 dex, implying that their distances would be underestimated by an overall factor of $1.22 \times 1.41 = 1.73$.

Cudworth (1974) derived distances for 56 northern galactic PN from a statistical parallax analysis. After separating the PN into optically thin and thick groups, he derived $K = 108.0$ for the thin PN. Therefore the Cudworth scale is only a factor of 1.01 larger than the Magellanic Cloud based scale that is used here. There are eight optically thin standard

PN in Table 6 in common with Cudworth's sample and for these we find a mean distance ratio (us/Cudworth) of 1.17 ± 0.22, consistent with the predicted ratio of 0.99. The absolute Hβ flux calibration for Cudworth's optically thick PN is, however, 0.51 dex fainter than the one adopted here, as some objects which we find optically thin [via the n_e(O II)] are included in his thick sample. This should lead to a mean factor of 1.8 difference in derived distances. For the 13 optically thick PN in Table 6 in common with Cudworth's sample, we find a mean distance ratio (us/Cudworth) of 1.64 ± 0.34.

Acker (1978) presented distances for 330 PN based on a synthesis of a variety of different methods. For the 19 thin PN in Table 6 in common with Acker's sample, we find a mean distance ratio (us/Acker) of 2.0 ± 0.6, while for the 20 optically thick PN in common with Acker's sample we find a mean distance ratio of 2.6 ± 1.2.

Milne (1982) based his radio flux scale for optically thick PN on the optically thick calibrations of Cudworth (1974) and Acker (1978). His equation (7) consequently yields distances which are smaller (by a factor of 2.1) than given by our equation (15). The optically thin calibration of Milne & Aller (1975) is the same as that of Cahn & Kaler (1971), discussed above.

Maciel & Pottasch (1980) derived distances to 121 galactic PN based on a mass–radius relation established for 21 PN whose distances had been determined by various means. The masses were derived assuming a constant $\epsilon = 0.60$, using the electron densities of Barker (1978); the resulting mass–radius relation was deemed to be valid for $0.01 < R < 0.4$ pc, i.e. none of the PN in our current sample would be optically thin according to this criterion. Maciel (1984) used this relation to derive distances (or distance limits) to over 400 PN. A comparison of our derived distances to the 13 optically thick PN in Table 6 in common with those of Maciel & Pottasch (1980) and Maciel (1984) yields a mean ratio (ours/theirs) of 2.52 ± 0.86. The same comparison for 15 optically thin PN from Table 6 yields a ratio of 2.23 ± 0.78.

Daub (1982) estimated distances to 299 galactic PN, using calibrators similar to those used by Acker (1978), having obtained a relation between ionized mass and radius similar to that of Maciel & Pottasch (1980). Only four of his 14 calibrator PN are in common with our sample, but their distances are lower, by a mean factor of 2.1 ± 0.3, than those derived here. The optically thin portion of Daub's fig. 1 corresponds to $K = 115.3$, similar to that adopted here, but optical thinness does not occur in his calibration until a radius corresponding to an rms nebular electron density of 1430 cm^{-3} [or n_e(O II) = 2250 cm^{-3}, if $\epsilon = 0.4$]. This transition density is a factor of 2 lower than given by the Magellanic Cloud calibration used here and consequently Daub's calibration will give lower distances for PN with densities between 2000 and 4500 cm^{-3}. The Hβ luminosity of a PN at the transition radius in Daub's calibration is 0.80 dex lower than adopted here, corresponding to a factor of 2.5 lower in derived distances. For the 19 optically thin PN in Table 6 in common with Daub, we obtain a mean distance ratio (us/Daub) of 2.3 ± 0.8, while for the 14 optically thick PN in Table 6 in common with Daub's sample the mean distance ratio is 3.2 ± 0.4.

Gathier *et al.* (1986a) have estimated H I absorption velocity kinematic distances for a number of galactic PN, of which seven are in common with our sample. Comparison of their distance limits (see column 6 of Table 6) with the distances derived here (column 5) shows agreement in all cases. For five of the seven PN, Gathier *et al.* (1986a) could only determine lower limits to the nebular distances. Gathier *et al.* (1986b) estimated distances to 12 galactic PN from the reddening–distance method, whereby the reddenings to nearby field stars as a function of distance are compared to the reddening determined for the PN. The early-type field stars used for the comparison mostly had apparent magnitudes brighter than 13.5 and few had derived distances exceeding 2.5 kpc. The method has to be confined to PN at very low galactic latitudes, since otherwise the sight-line to the PN soon leaves the galactic dust layer. For the only standard PN in common (NGC 6565), we derive a distance of 7.7 kpc and a height above the galactic plane of 0.62 kpc; Gathier *et al.* (1986b) estimated a dust extinction distance of 1.0 kpc. Kaler & Lutz (1985) estimated dust extinction distances to seven PN. For the only PN in common, NGC 7026, they derived a distance of 1.5 ± 0.8 kpc, compared to the dust extinction distance of 2.2 ± 0.7 kpc derived by Solf & Weinberger (1984) and the distance of 3.4 ± 0.7 kpc derived here. We conclude that the reddening versus distance method is useful in providing lower limits to PN distances but that lack of distant comparison stars, coupled with the position of many PN well above the galactic dust layer, makes it difficult to set upper distance limits by this method.

Weidemann (1977) argued that if the narrow mass range found for white dwarfs, centred on $0.6 M_\odot$, also applied to the central stars of PN, the distance scale adopted by Cahn & Kaler (1971) should be increased by a factor of 1.3, which is close to the factor of 1.41 given by the Magellanic Cloud scale used here. Schoenberner (1981) adopted this factor of 1.3 increase to the Cahn & Kaler (CK) scale (as well as lower reddenings than those of CK, thus giving a further increase in adopted distances relative to those of CK). He plotted central star absolute magnitudes versus evolutionary ages since leaving the asymptotic giant branch (assumed to be equal to the nebular expansion age), in order to derive the central star masses via a comparison with theoretical evolutionary tracks. He recovered a highly peaked central star mass distribution, centred on $0.6 M_\odot$, with a high-mass tail. Heap & Augensen (1987) used the 'short' distance scale of Daub (1982) for a similar study, this time using ultraviolet central star magnitudes. They found a broader distribution of PN central star masses than Schoenberner (1981), with a median mass of $0.65 M_\odot$ and with 56 per cent of the masses above $0.64 M_\odot$, compared to only 27 per cent in the case of Schoenberner.

Because more massive nuclei are predicted to cool faster to faint magnitudes, the effect of underestimating distances when using this method is to overestimate central star masses. Weidemann (1989) pointed this out and showed that, if instead of Daub's distances the Magellanic Cloud PN distance calibrations of Barlow (1987; virtually identical to those adopted here) were used for Heap & Augensen's sample, the effect was to recover a sharply peaked central star mass distribution, with 77 per cent having masses below $0.64 M_\odot$; for a local ensemble of 22 PN, the average central star mass became $0.60 M_\odot$ and the median mass was $0.59 M_\odot$. This agrees with the average central star mass of

$0.59 \pm 0.02 M_{\odot}$ found by Walton *et al.* (1991) for 14 Magellanic Cloud PN. It is worth noting that for central star effective temperatures less than 70 000 K, the stellar masses derived from luminosity versus effective temperature comparisons with theoretical evolutionary tracks will decrease if the adopted distance is decreased, whereas masses derived from M_V versus expansion time-scale considerations will increase. In principle, agreement between the two methods will be obtained for only one distance. We can consider the case of IC 418 as an example. From ionization structure modelling of IC 418, Middlemass (1988) obtained a stellar luminosity equivalent to $2850 L_{\odot}$ from a 40 000-K blackbody at 1 kpc, while Hoare (1990) obtained $3150 L_{\odot}$ at 1 kpc for the case of the Mendez *et al.* (1988) non Local Thermodynamic Equilibrium (NLTE) model with $T_{\rm eff} = 36\,000$ K and $\log g = 3.3$. We adopt a mean of $3000 L_{\odot}$ at 1 kpc. Using the Daub (1982) distance of 0.412 kpc, Heap & Augensen (1987) derived an $M(\lambda 1300)$, $t_{\rm exp}$ central star mass of $0.66 M_{\odot}$, from comparison with tracks based on the evolutionary models of Schoenberner (1983). However, the stellar luminosity of $510 L_{\odot}$ that corresponds to a distance of 0.412 kpc would put the central star far below the L, $T_{\rm eff}$ evolutionary track of even the 0.546-$M_{\odot}$ model of Schoenberner (1983). Using the distance of 1.25 kpc to IC 418 derived here (Table 8), the central star has a luminosity of $4690 L_{\odot}$, an L, $T_{\rm eff}$ mass of $0.58 M_{\odot}$, and an $M(\lambda 1300)$, $t_{\rm exp}$ mass of $0.60 M_{\odot}$. Therefore a distance of 1.25 kpc gives much greater consistency between the two methods.

Mendez *et al.* (1988, 1990) have derived central star distances using NLTE atmospheric analyses of high-resolution spectra from which $\log g$ and $T_{\rm eff}$ were derived. Comparison of these two parameters with those given by theoretical evolutionary tracks allows the central star masses and ultimately the distances to be derived. There are seven PN common to our sample and those of Mendez *et al.* Of the seven central stars, three have absorption-line O-type spectra and four have Of-type spectra (spectral types are listed in Table 2). For the three O-type stars the mean ratio of the derived distances (us/Mendez *et al.*) is 1.00 ± 0.27, while for the four Of stars the mean ratio is 0.71 ± 0.24. For the three O stars the mean mass derived by Mendez *et al.* (1988, 1990) was $0.70 \pm 0.02 M_{\odot}$, whereas for the four Of stars the mean derived mass was $0.81 \pm 0.07 M_{\odot}$. Mendez *et al.* also estimated distances to NGC 6543 and 6572 on the assumption that their Of–WR central stars also had masses of $0.8 M_{\odot}$ (however, we note that for Magellanic Cloud PN, Monk, Barlow & Clegg (1990) found no difference between the mean mass of $0.59 M_{\odot}$ derived for four WR central stars and the mean mass of nine non-WR central stars). The resulting mean distance ratio (us/Mendez *et al.*) is 0.55 ± 0.12. We believe that these trends are due to the surface gravities of the absorption-line O stars and the emission-line Of stars being underestimated by the plane-parallel NLTE models used by Mendez *et al.* In cases where the surface gravity is underestimated, their method will overestimate both the mass and distance of the central star. For example, in the case of the Of central star of IC 418, Mendez *et al.* (1988) derive a mass of $0.77 M_{\odot}$ and a distance of 2.0 kpc whereas, as discussed in the previous paragraph, the distance of 1.25 kpc given by the Magellanic Cloud calibration gives a consistent mass of 0.58–$0.60 M_{\odot}$ from each of the independent L, $T_{\rm eff}$ and $M(\lambda 1300)$, $t_{\rm exp}$ methods. Hubeny, Heap & Altner (1991) have argued, on the basis of an analysis of the ultraviolet spectra of a subdwarf O star and a massive O star, that significant microturbulence must be accounted for when fitting the absorption-line profiles of hot stars. They show that the incorporation of microturbulence into the NLTE modelling of line profiles will lead to an increase in the derived surface gravity and thus, in the case of PN central stars, to a decrease in the derived stellar mass. A mean increase of less than 0.2 dex in derived $\log g$s is needed in order to reduce the mean mass from 0.65 to $0.59 M_{\odot}$ for the 14 absorption-line O stars in the sample of Mendez *et al.* (1988). A larger increase in the derived $\log g$s would be needed in order to reduce the mean mass of the seven emission-line Of stars in their sample from 0.77 to $0.6 M_{\odot}$. A reduction in the PN central star masses derived from NLTE absorption-line fitting would also help to eliminate the serious discrepancy found by McCarthy *et al.* (1990) between the central star evolutionary ages and the nebular expansion ages.

The calibrations used here can also be applied to Galactic Bulge PN in order to compare the resulting mean distance with current estimates for the distance to the Galactic Centre. From the Middlemass (1989) sample of bulge PN with [O II] electron densities and reliable radio fluxes, the 13 optically thick standard PN yield a mean distance of 9.27 ± 1.36 kpc (there were only five optically thin standard PN in the Middlemass sample and they yield a mean distance of 9.8 ± 3.5 kpc). For a distance to the Galactic Centre of 8.5 ± 1.1 kpc (Kerr & Lynden-Bell 1986), the implied mean Hβ luminosity of these optically thick bulge PN would be 0.075 dex smaller than that for Magellanic Cloud PN. Application of the Cudworth (1974) Hβ flux calibration for optically thick PN to this sample yields a distance of only 5.15 kpc to the Galactic Centre.

Finally, we can compare the distances derived for two of the PN in our sample with the VLA expansion distances measured by Masson (1989a,b). For NGC 7027, we obtain 0.78 ± 0.11 kpc, compared to 0.88 ± 0.15 kpc derived by Masson (1989a), while for NGC 6572 we obtain 1.60 ± 0.22 kpc, compared to 1.7 kpc obtained by Masson (1989b; although the short VLA time baseline gives a large formal uncertainty of $+6.1$, -0.8 kpc in the latter case).

The integrated [O II] doublet ratio results of the present paper pertain primarily to northern hemisphere PN. The programme has recently been extended to encompass a survey of PN in the southern hemisphere, for which integrated [S II] 6716, 6731-Å ratios, as well as [O II] 3726, 3729-Å ratios, will be reported for 65 objects (Kingsburgh & English, in preparation).

ACKNOWLEDGMENTS

We thank PATT for allocations of telescope time. The data presented in this paper were obtained at the Anglo-Australian Telescope, which is operated by the Anglo-Australian Observatory, and at the Jacobus Kapteyn Telescope, which is operated by the Observatorio de la Roque de los Muchachos. We thank the staff at these telescopes for their support. We would also like to thank J. R. Deacon for his assistance at the JKT and P. J. Storey for his effort on the ELF package.

REFERENCES

Aaquist, O. B. & Kwok, S., 1990. *Astr. Astrophys. Suppl.*, **84,** 229.
Aaquist, O. B. & Kwok, S., 1991. *Astrophys. J.*, **378,** 599.
Abell, G. O., 1966. *Astrophys. J.*, **144,** 259.
Acker, A., 1978. *Astr. Astrophys. Suppl.*, **33,** 367.
Acker, A., Chopinet, M., Marcourt, J., Ochsenbein, F. & Rogues, J. M., 1982. *Catalogue of the Central Stars of Planetary Nebulae,* Publ. Speciale du C.D.S. No. 3, Observatoire de Strasbourg.
Adams, S., 1983. *PhD thesis,* University of London.
Adams, S., Seaton, M. J., Howarth, I. D., Auriere, M. & Walsh, J. R., 1984. *Mon. Not. R. astr. Soc.*, **207,** 471.
Allen, D., 1973. *Observatory,* **93,** 28.
Aller, L. H. & Czyzak, S. J., 1979. *Astrophys. Space Sci.*, **62,** 397.
Aller, L. H. & Czyzak, S. J., 1983. *Astrophys. J. Suppl.*, **51,** 211.
Aller, L. H. & Keyes, C. D., 1987. *Astrophys. J. Suppl.*, **65,** 405.
Aller, L. H., Keyes, C. D. & Czyzak, S. J., 1981. *Astrophys. J.*, **250,** 596.
Aller, L. H., Keyes, C. D. & Feibelman, W. A., 1988. *Publs astr. Soc. Pacif.*, **100,** 192.
Altschuler, D. R., Schneider, S. E., Giovanardi, C. & Silverglate, P. R., 1986. *Astrophys. J. Lett.*, **305,** L85.
Barker, T., 1978. *Astrophys. J.*, **219,** 914.
Barlow, M. J., 1987. *Mon. Not. R. astr. Soc.*, **227,** 161.
Bignell, R. C., 1983. In: *Planetary Nebulae, IAU Symp. No. 103,* p. 69, ed. Flower, D., Reidel, Dordrecht.
Cahn, J. H. & Kaler, J. B., 1971. *Astrophys. J. Suppl.*, **22,** 319.
Carrasco, L., Serrano, A. & Costero, R., 1983. *Rev. Mex. Astr. Astrofis.*, **8,** 187.
Chu, Y. H., Jacoby, G. H. & Arendt, R., 1987. *Astrophys. J. Suppl.*, **64,** 529.
Clegg, R. E. S., 1987. *Mon. Not. R. astr. Soc.*, **229,** 31P.
Clegg, R. E. S., Seaton, M. J., Peimbert, M. & Torres-Peimbert, S., 1983. *Mon. Not. R. astr. Soc.*, **188,** 229.
Cudworth, K. M., 1974. *Astr. J.*, **79,** 1384.
Daub, C. T., 1982. *Astrophys. J.*, **260,** 612.
Dinerstein, H. L., Carr, J. S. & Harvey, P. M., 1988. *Astrophys. J. Lett.*, **327,** L27.
Dopita, M. A. & Meatheringham, S. J., 1991. *Astrophys. J.*, **367,** 115.
Flower, D. R., 1980. *Mon. Not. R. astr. Soc.*, **193,** 511.
Gathier, R., Pottasch, S. R. & Pel, J. W., 1986a. *Astr. Astrophys.*, **157,** 171.
Gathier, R., Pottasch, S. R. & Goss, W. M., 1986b. *Astr. Astrophys.*, **157,** 191.
Gathier, R., Pottasch, S. R., Goss, W. M. & van Gorkom, J. H., 1983. *Astr. Astrophys.*, **128,** 325.
Gutierrez-Moreno, A., Moreno, H. & Cortes, G., 1985. *Publs astr. Soc. Pacif.*, **97,** 397.
Harrington, J. P. & Feibelman, W. A., 1983. *Astrophys. J.*, **265,** 258.
Heap, S. R. & Augensen, H. J., 1987. *Astrophys. J.*, **313,** 268.
Hoare, M. G., 1990. *Mon. Not. R. astr. Soc.*, **244,** 193.
Howarth, I. D. & Murray, J., 1988. *SERC STARLINK User Note No. 50,* Rutherford Appleton Laboratory.
Hubeny, I., Heap, S. R. & Altner, B., 1991. *Astrophys. J. Lett.*, **377,** L33.
Hummer, D. G. & Storey, P. J., 1987. *Mon. Not. R. astr. Soc.*, **224,** 801.
Jewitt, D. C., Danielson, G. E. & Kupferman, P. N., 1986. *Astrophys. J.*, **302,** 727.
Johnson, H. M., Kulkarni, S. R. & Goss, W. M., 1991. *Astrophys. J. Lett.*, **382,** L89.
Kaler, J. B., 1978. *Astrophys. J.*, **220,** 887.
Kaler, J. B., 1980. *Astrophys. J.*, **239,** 78.
Kaler, J. B. & Lutz, J. H., 1985. *Publs astr. Soc. Pacif.*, **97,** 700.
Kaler, J. B., Shaw, R. & Kwitter, K., 1990. *Astrophys. J.*, **359,** 392.
Kerr, F. J. & Lynden-Bell, D., 1986. *Mon. Not. R. astr. Soc.*, **221,** 1023.
Kohoutek, P. & Martin, W., 1981. *Astr. Astrophys. Suppl.*, **44,** 325.
Lutz, J. H., 1974. *Publs astr. Soc. Pacif.*, **86,** 888.
Lutz, J. H., 1989. *Planetary Nebulae, IAU Symp. No. 131,* p. 65, ed. Torres-Peimbert, S., Kluwer, Dordrecht.
Maciel, W. J., 1984. *Astr. Astrophys. Suppl.*, **55,** 253.
Maciel, W. J. & Pottasch, S. R., 1980. *Astr. Astrophys.*, **88,** 1.
Mallik, D. C. V. & Peimbert, M., 1988. *Rev. Mex. Astr. Astrofis.*, **16,** 111.
Martin, W., 1981. *Astr. Astrophys.*, **98,** 328.
Masson, C. R., 1989a. *Astrophys. J.*, **336,** 294.
Masson, C. R., 1989b. *Astrophys. J.*, **346,** 243.
McCarthy, J. K., Mould, J. R., Mendez, R. H., Kudritzki, R. P., Husfield, D., Herrero, A. & Groth, H. R., 1990. *Astrophys. J.*, **351,** 230.
Meatheringham, S. J., Dopita, M. A. & Morgan, D. H., 1988. *Astrophys. J.*, **329,** 166.
Mendez, R. H., 1991. *Evolution of Stars: The Photospheric Abundance Connection, IAU Symp. No. 145,* p. 375, eds Michaud, G. & Tutukov, A., Reidel, Dordrecht.
Mendez, R. H., Herrero, A. & Manchado, A., 1990. *Astr. Astrophys.*, **229,** 152.
Mendez, R. H., Kudritzki, R. P., Herrero, A., Husfield, D. & Groth, H. G., 1988. *Astr. Astrophys.*, **190,** 113.
Mendoza, C., 1983. *Planetary Nebulae, IAU Symp. No. 103,* p. 143, ed. Flower, D. R., Reidel, Dordrecht.
Middlemass, D., 1989. *PhD thesis,* University of London.
Middlemass, D., 1990. *Mon. Not. R. astr. Soc.*, **244,** 294.
Miller, J. S., 1971. *Astrophys. J. Lett.*, **165,** L101.
Milne, D. K., 1982. *Mon. Not. R. astr. Soc.*, **200,** 51P.
Milne, D. K. & Aller, L. H., 1975. *Astr. Astrophys.*, **38,** 183.
Milne, D. K. & Aller, L. H., 1982. *Astr. Astrophys. Suppl.*, **50,** 209.
Minkowski, R., 1965. In: *Galactic Structure,* p. 321, eds Blaauw, A. & Schmidt, M., University of Chicago Press, Chicago.
Monk, D. J., Barlow, M. J. & Clegg, R. E. S., 1990. *Mon. Not. R. astr. Soc.*, **242,** 457.
O'Dell, C. R., 1962. *Astrophys. J.*, **135,** 371.
O'Dell, C. R., 1963. *Astrophys. J.*, **138,** 293.
Oster, L., 1961. *Rev. Mod. Phys.*, **33,** 525.
Osterbrock, D. E., 1989. *Astrophysics of Gaseous Nebulae and Active Galactic Nuclei*, University Science Books, Mill Valley, CA.
Peimbert, M., 1978. *Planetary Nebulae: Observations and Theory, IAU Symp. No. 76,* p. 215, ed. Burton, W. B., Reidel, Dordrecht.
Peimbert, M., 1990. *Rep. Prog. Phys.*, **53,** 1559.
Peimbert, M. & Torres-Peimbert, S., 1987. *Rev. Mex. Astr. Astrofis.*, **14,** 540.
Perek, L., 1971. *Bull. astr. Inst. Czech.*, **22,** 103.
Perek, L. & Kohoutek, L., 1967. *Catalogue of Galactic Planetary Nebulae,* Academia Publ. House of the Czechoslovak Academy of Sciences, Prague.
Pradhan, A. K., 1976. *Mon. Not. R. astr. Soc.*, **177,** 31.
Schoenberner, D., 1981. *Astr. Astrophys.*, **103,** 119.
Schoenberner, D., 1983. *Astrophys. J.*, **272,** 708.
Seaquist, E. R. & Davis, L. E., 1983. *Astrophys. J.*, **274,** 659.
Seaton, M. J., 1968. *Astrophys. Lett.*, **2,** 55.
Seaton, M. J. & Osterbrock, D. E., 1957. *Astrophys. J.*, **125,** 66.
Shaw, R. & Kaler, J. B., 1985. *Astrophys. J.*, **295,** 537.
Shaw, R. & Kaler, J. B., 1989. *Astrophys. J. Suppl.*, **69,** 495.
Shklovsky, I. S., 1956. *Astr. Zh.*, **33,** 222.
Shortridge, K., 1989. *SERC STARLINK User Note No. 86,* Rutherford Appleton Laboratory.
Smith, L. F. & Aller, L. H., 1969. *Astrophys. J.*, **157,** 1245.
Solf, J. & Weinberger, R., 1984. *Astr. Astrophys.*, **130,** 269.
Tamura, S. & Shaw, R. A., 1987. *Publs astr. Soc. Pacif.*, **99,** 1264.
Torres-Peimbert, S. & Peimbert, M., 1977. *Rev. Mex. Astr. Astrophys.*, **2,** 181.
Viadana, L. & de Freitas Pacheco, J. A., 1985. *Rev. Bras. Fis.*, **15,** 70.
Vorontsov-Velyaminov, B. A., 1934. *Z. Astrophys.*, **8,** 195.
Walton, N. A., Barlow, M. J., Clegg, R. E. S. & Monk, D. J., 1991.

The Magellanic Clouds, IAU Symp. No. 146, p. 337, eds Haynes, R. & Milne, D., Kluwer, Dordrecht.
Webbink, R. H., 1985. *Dynamics of Star Clusters, IAU Symp. No. 113,* p. 541, eds Goodman, J. & Hut, P., Reidel, Dordrecht.
Webster, B. L., 1969. *Mon. Not. R. astr. Soc.*, **143,** 79.
Webster, B. L., 1983. *Publs astr. Soc. Pacif.*, **95,** 610.
Webster, B. L., 1988. *Mon. Not. R. astr. Soc.*, **230,** 377.
Weidemann, V., 1977. *Astr. Astrophys.*, **61,** L27.
Weidemann, V., 1989. *Astr. Astrophys.*, **213,** 1989.
Wood, P. R., Bessel, M. S. & Dopita, M. A., 1986. *Astrophys. J.*, **311,** 632.
Wood, P. R., Meatheringham, S. J., Dopita, M. A. & Morgan, D. H., 1987. *Astrophys. J.*, **320,** 178.
Zanstra, H., 1931. *Z. Astrophys.*, **2,** 329.
Zeippen, C. J., 1982. *Mon. Not. R. astr. Soc.*, **198,** 111.
Zijlstra, A. A., Pottasch, S. R. & Bignell, C., 1989. *Astr. Astrophys. Suppl.*, **79,** 329.

APPENDIX: RMS ELECTRON DENSITIES AND FILLING FACTORS

For a PN with a known distance and angular diameter, we can derive n_e(rms) from the radio free–free flux if the electron temperature is also known. The free–free continuum emitted by electrons during Coulomb collisions with positive ions (H^+, He^+ and He^{++}) can be derived following Oster (1961). At a frequency $\nu = 5$ GHz, n_e(rms) takes the form

$$n_e^2(\mathrm{rms}) = 2.264 \times 10^8 \frac{S_\nu(5\ \mathrm{GHz})}{D\theta^3} \frac{t^{1/2}}{(1.5 \ln t + 9.2)} \times \frac{(1 + y^+ + 4y^{++})}{(1 + y^+ + 2y^{++})}, \quad \text{(A1)}$$

where n_e(rms) is in cm^{-3}, S_ν(5 GHz) is in mJy, $t = T_e/10^4$ K, D is the distance in kpc and θ is the nebular angular radius in arcsec, $y^+ = n(He^+)/n(H^+)$ and $y^{++} = n(He^{++})/n(H^+)$. n_e(rms) should always be less than or equal to n_e(FL) due to the density inhomogeneities that exist in nebulae. The forbidden-line (FL) flux is weighted towards the regions of highest emission measure and accordingly the highest densities; thus the derived forbidden-line densities will be higher than the average density over the whole volume of the nebula contained within its measured angular diameter. These density fluctuations have traditionally been described by ϵ, the filling factor, which is defined as the square of the ratio of the rms and forbidden-line densities:

$$\epsilon = \left[\frac{n_e(\mathrm{rms})}{n_e(\mathrm{FL})}\right]^2, \quad \text{(A2)}$$

i.e. the PN has a fraction ϵ of its volume filled with material at a density n_e(FL) which contributes to the mass, emission, etc., while the rest of its volume is empty. The filling factor ϵ accounts for both the macroscopic and microscopic density fluctuations within the nebula.

We have derived filling factors for our current sample of PN using the [O II] doublet ratio densities and distances listed in Tables 6–8. The dominant source of error for ϵ is the error in the adopted angular radius, since ϵ is proportional to θ^{-3}. Sensitive CCD surveys have revealed that many PN have outer haloes surrounding brighter cores. Since even the inner bright cores often have smoothly varying brightness distributions, the question arises as to where to define the outer angular radius θ. Published optical and radio diameters tend to differ, often by large factors. The radio diameters are usually smaller, presumably due to a smaller dynamic range. Yet a change of θ by a factor of 2 will cause ϵ to change by a factor of 8. Whenever possible, we have adopted optical diameters, principally from the CCD survey of Chu *et al.* (1987). However, VLA radio diameters measured by Zijlstra *et al.* (1989) or by Aaquist & Kwok (1990) have had to be adopted in the cases of 19 of the PN. In the cases of PN which are not symmetric, we have adopted geometric means of the major and minor axis diameters. Tables A1, A2 and A3 present n_e(O II), n_e(rms), the filling factor ϵ, the nebular angular radius θ (from the references given in Tables 1 and 5) and the absolute nebular radius R, for the 'standard' PN, the Type I PN and the LE PN, respectively. Fig. A1 plots ϵ versus R for objects whose integrated [O II] doublet ratios in Table 2 are not qualified by colons.

12 out of 52 PN were found to have $\epsilon > 1$. Within the error limits of the [O II] doublet ratios, $\epsilon \simeq 1$ for M 1-5 and NGC 6572. The angular diameter of Sn 1 is noted as uncertain by Aaquist & Kwok (1990). M 1-8 and He 2-108 do not have integrated flux measurements. M 1-8 is near the low-density limit of the 3726/3729 ratio, so that small changes in the ratio could lead to large changes in the derived n_e(O II). The [O II] doublet ratio found for IC 5117 is consistent within its errors with being at the high-density limit. For it, and for the six remaining PN for which $\epsilon > 1$ is obtained (NGC 6644, Vy 2-2, IC 4997, NGC 7027, Me 2-2 and Hb 12), $n_e(\mathrm{rms}) > 1.5 \times 10^4\ \mathrm{cm}^{-3}$ is derived, so that the density derived from the [O II] 3726 + 3729/7325 ratio is likely to be more appropriate for deriving a filling factor than that obtained from the 3726/3729 ratio (see Section 4.4). As discussed in more detail in Section 5.2 for several of these objects, the fact that their 3726/3729 doublet ratios are below the high-density limit appears to be due to the presence of extended lower density material around their dense ionized cores.

A recent study of filling factors in PN by Mallik & Peimbert (1988) indicated relatively small filling factors and the existence of an ϵ–R relation, so that at larger radii smaller ϵs were encountered. They postulated that a fast wind from the central star that is responsible for the central cavity produces clumping within the nebula via Rayleigh–Taylor instabilities.

For objects in common to this survey and that of Mallik & Peimbert, we find somewhat larger filling factors. Our distances are generally larger than the mainly dust-extinction distances adopted by Mallik & Peimbert, but inspection of equation (A1) shows that this factor alone would lead us to derive smaller, not larger, filling factors. The main difference seems to lie in the use of different n_e(FL)s. Mallik & Peimbert adopted n_e(FL) from a compilation of literature sources of [O II], [S II], [Cl III] and [Ar IV] ratios. These were rarely integrated ratios and are not appropriately tracing the emitting mass (as discussed in Section 4.4, the [Ar IV] ratio is not a suitable mass tracer anyway).

In Fig. A1 we plot the filling factor ϵ versus the ionized nebular radius R for the 'standard' PN in our own sample.§

§Note that a selection effect is present in Fig. A1; objects whose densities are above the high-density limit of the [O II] doublet ratio have underivable filling factors.

Table A1. Rms electron densities, filling factors and radii for 'standard' PN.

	Object	n_e(OII)[b] (cm^{-3})	n_e(RMS) (cm^{-3})	θ (″)	ϵ	R (pc)
*	Hu 1-1	1320	920	5	0.49	0.15
	IC 351	4470:	1160	3.5	0.067	0.20
	IC 2003	13200:	960	5.7	0.005	0.23
	M 1-5	12300:	12900	1.2	1.09	0.037
	IC 2149	(3790)	2580	6.1	0.46	0.11
*	IC 2165	5010	3260	5	0.40	0.11
*	J 900	3980	3950	3	0.98	0.085
	M 1-8	(140:)	520	9.2	13	0.11
	M 3-1	(1070)	780	5.5	0.54	0.16
*	NGC 2392	1450	790	18	0.30	0.18
	M 3-6	(3020)	1370	5.5	0.21	0.16
*	NGC 3242	2290	1130	22	0.25	0.16
*	IC 3568	2140	1210	6.8	0.18[c]	0.16
	NGC 5307	(3800)	1170	6.5	0.094	0.19
	NGC 5873	(6460)	1600	3.5	0.061	0.17
	NGC 5882	(4370)	2780	3.5	0.40	0.10
*	Me 2-1	1820	1400	3.5	0.59	0.13
*	IC 4593	1660	1470	6.5	0.79	0.12
	Sn 1[a]	1290:	2860:	1.5	4.91:	0.071:
*	NGC 6210	5250	2730	6.5	0.27	0.11
	IC 4642	(980)	700	8.2	0.51	0.17
*	NGC 6543	3890	2480	11.7	0.41	0.11
*	NGC 6565	2570	980	5	0.14	0.19
*	NGC 6572	6610	7680	7	1.35	0.051
	NGC 6644	5370	14300	1.8	7.08	0.038
	NGC 6751	(1050)	590	10	0.31	0.19
	IC 4846	hdl	6340	1.5	–	0.060
	Vy 2-2	10500	47000	0.2	>>1	0.004
	NGC 6803	hdl	4350	2.8	–	0.077
	NGC 6807	hdl	32600	0.4	–	0.021
*	NGC 6818	2240	1530	11	0.47	0.13
	NGC 6833[a]	hdl	71600	0.25	–	0.013
*	NGC 6886	5750	5360	2.5	0.87	0.075
*	NGC 6891	3720	1830	5.5	0.24	0.14
	IC 4997[a]	15500	69000	0.8	20	0.014
*	NGC 7009	4350	1470	14.7	0.11	0.16
*	NGC 7026	3240	770	11.3	0.057	0.24
	NGC 7027[a]	13300	27000	14.2	4.12	0.027
	IC 5117	21900:	53200	0.8	5.90	0.014
*	NGC 7662	2950	1350	16.5	0.21	0.16

Table A2. Rms electron densities, filling factors and radii for Type I PN.

Object	n_e(OII)[b] (cm^{-3})	n_e(RMS) (cm^{-3})	θ (″)	ϵ	R (pc)
K 3-67	30200:	9450	1.1	0.098	0.051
M 1-13	(890)	300	7.5	0.11	0.34
M 3-3	(330)	240	6.2	0.53	0.056
NGC 2452	(1170)	560	9.4	0.23	0.25
He 2-111	(780)	340	15.7	0.19	0.31
He 2-112	(2510)	860	7.3	0.12	0.24
NGC 6445	1000	820	18	0.67	0.19
Hu 1-2[a]	11200	4520	4.2	0.16	0.10
Me 2-2[a]	14100	25600	0.6	3.29	0.026

Table A3. Rms electron densities, filling factors and absolute radii for LE PN.

Object	n_e(OII) (cm^{-3})	n_e(RMS) (cm^{-3})	θ (″)	ϵ	R (pc)
NGC 40[a]	1200	590	24.3	0.24	0.27
IC 418	13200	12400	6.2	0.88	0.037
He 2-108	(630)	1200	5.5	3.66	0.10
Hb 12[a]	4900	234000	0.4	>>1	0.0059

Notes to Tables A1, A2 and A3.
[a]Indicates the 5-GHz flux was unreliable or is optically thick in the free–free continuum, hence an $I(H\beta)$ derived via equation (7) was used to derive n_e(rms); [b]quantities in parentheses have been derived from an n_e(O II) which does not represent an integrated value [i.e. the adopted n_e(O II) is a straight or weighted mean of spatial increments which do not encompass the entire nebula]; [c]see Section 5.2 for a discussion of the filling factor for IC 3568. *Indicates that the object has been plotted in Fig. A1. These objects have n_e(O II) derived from a high signal-to-noise integrated 3726,29-Å doublet ratio (i.e. those without a colon) and n_e(rms) derived from a reliable 5-GHz or $F(H\beta)$ measurement.

Fig. A1 shows a linear–linear plot, for comparison with the results of Mallik & Peimbert (1988), while Fig. A2 is a log–log plot of the optically thin PN. The optically thin PN (open symbols) and the optically thick PN (filled symbols) appear displaced from each other in Fig. A1. This may be due to the fact that for an optically thick PN the ionized nebular radius is smaller than the total nebular radius. Allowance for the larger true radii of optically thick PN should move their points to the right in Fig. A1, closer to the points for the optically thin nebulae. The mean filling factor found for the 14 optically thin 'standard' PN plotted in Fig. A1 is $\epsilon = 0.40 \pm 0.28$. The mean radius of five 'transition' PN (i.e. those with $3900 \lesssim n_e \lesssim 5200$ cm^{-3}) is 0.11 pc, although the range in radius spanned by these objects is 0.085–0.16 pc. The fit to the trend shown by the filling factors of the 14 optically thin nebulae plotted in Fig. A2 yields a slope of -2.62 ± 0.41 $\{\epsilon = 0.85(R/0.1\text{ pc})^{-2.62}$, where $R = \theta D$ and D is the distance determined via the [O II] method$\}$.

In Figs A1 and A2 there is a trend for ϵ to decrease as the nebular radius increases, as suggested by Mallik & Peimbert (1988) amongst others. We argue here, however, that such an effect results merely from the observational uncertainties associated with the PN angular diameters. Equations (A1) and (A2) imply a steep inverse dependence of the derived ϵ on the adopted angular radius θ. We can simulate the effects

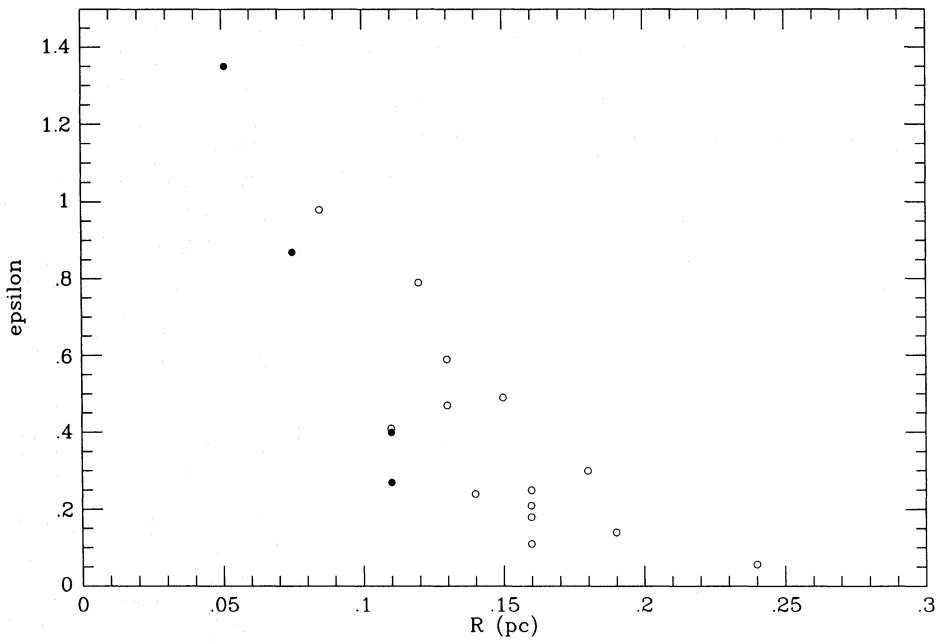

Figure A1. Filling factor ϵ versus radius R (pc) for 'standard' PN. 'Standard' PN are defined as non-Type I and non-low-excitation, where low-excitation PN have $I(\text{O III } 5007) < I(\text{H}\beta)$. Only objects with integrated [O II] 3726,29-Å doublet ratios which are not qualified by a colon in Table 2 are plotted (i.e. those marked with an asterisk in Table A1). Filled circles are optically thick nebulae and open circles are optically thin nebulae. Objects with $D_{\text{thin}} < D_{\text{thick}}$ are optically thin; objects with $D_{\text{thick}} < D_{\text{thin}}$ are optically thick.

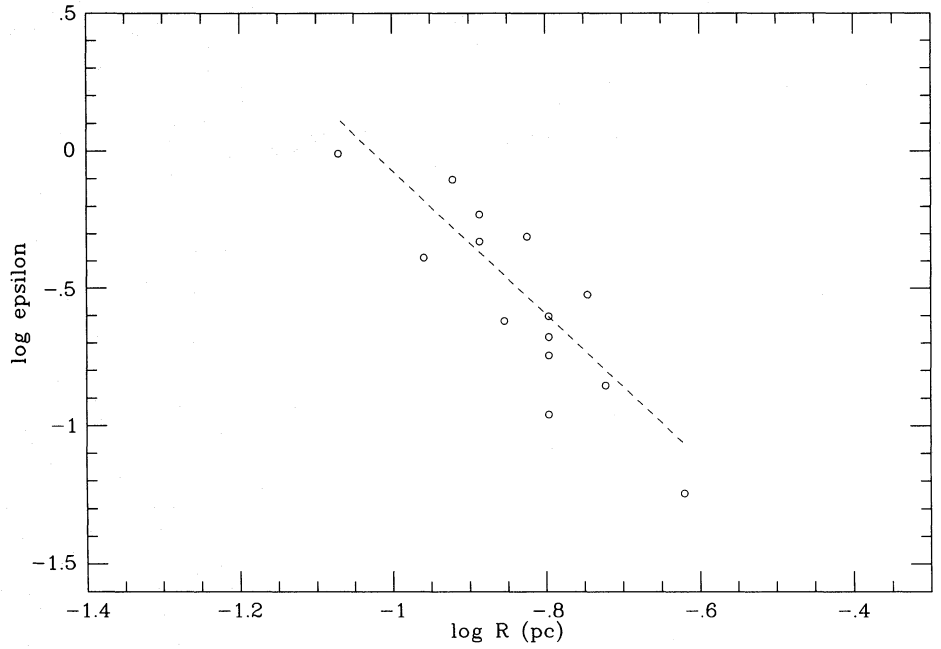

Figure A2. Log ϵ versus log R (pc) for the optically thin 'standard' PN. A least-squares fit yields a slope of -2.62 ± 0.41 for these objects.

of random observational errors of less than a factor of 2 in the adopted angular diameters. Let us consider a standard 'test' PN which has just become optically thin (i.e. is now completely ionized). An initial $n_e(\text{O II})$ of 5000 cm^{-3} will drop as R^{-3} as the nebula expands at constant M_H and ϵ. To try to estimate the effects of uncertainties in the angular diameters, let us examine the relationship between $n_e(\text{O II})$ and R, adopting a constant ϵ, then apply random uncertainties to R, consistent with a maximum uncertainty of a factor of 2 in the observed angular radii. Solving equation (7) for $I(\text{H}\beta)$ and substituting in equation (9) establishes the following straightforward relation between $n_e(\text{O II})$ and R:

$$R(\text{pc}) = 1.33 \left[\frac{1}{\epsilon n_e(\text{O II})} \right]^{1/3}, \qquad \text{(A3)}$$

where the average values for the 'standard' PN in this sample, $t=1.13$ and $\gamma=1.122$, have been used, along with $M_{\rm H}=0.217M_{\odot}$. For a given ϵ, we can allow this PN to expand and evaluate its R as a function of $n_{\rm e}$(O II). We took 'test' nebulae with six different values of ϵ ($\epsilon=0.1$, 0.2, 0.4, 0.45, 0.8 and 0.9) and calculated R at $n_{\rm e}$(O II)$=5000$, 4000, 3000, 2000 and 1000 cm^{-3} for each ϵ (i.e. within the same [O II] density range as the PN plotted in Figs A1 and A2). Random scatter was applied to each R by multiplication or division by a random number between 1.0 and 2.0 (generated by an HP15C calculator), allowing an 'observed' R ($R_{\rm obs}$) to be estimated. The decision to multiply or divide by

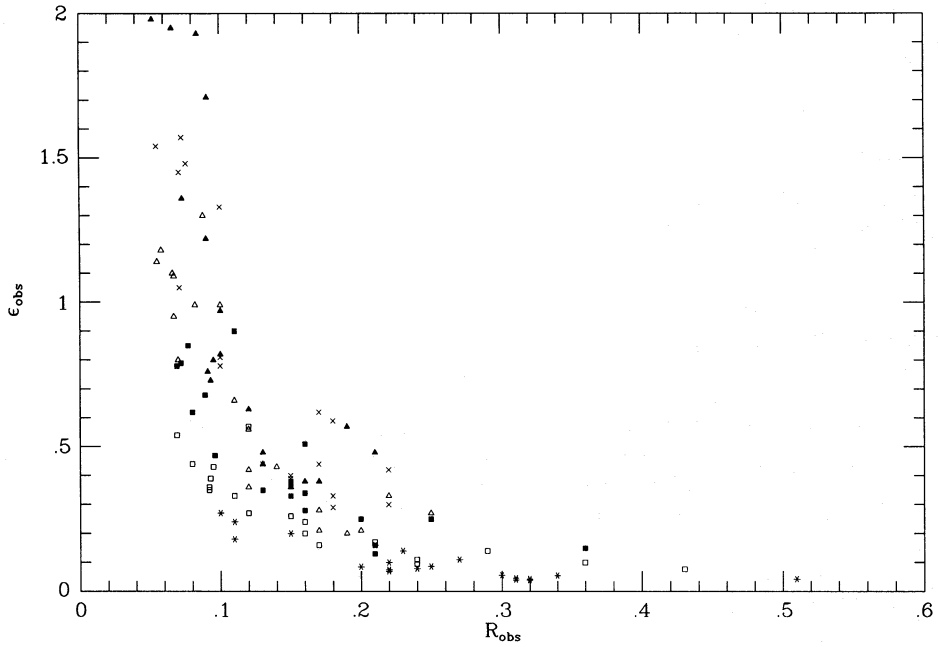

Figure A3. $\epsilon_{\rm obs}$ versus $R_{\rm obs}$ for 'simulated' optically thin standard PN which have been allowed to expand at constant ionized mass with a variety of constant filling factors ϵ, where random errors have been applied to the radius, yielding an 'observed' radius $R_{\rm obs}$ which was then used to derive an 'observed' filling factor $\epsilon_{\rm obs}$. See the Appendix for details of the randomization procedure. Symbols for the various filling factor sequences are as follows: filled triangles, $\epsilon=0.9$; crosses, $\epsilon=0.8$; open triangles, $\epsilon=0.45$; filled squares, $\epsilon=0.4$; open squares, $\epsilon=0.2$; and skeletal stars, $\epsilon=0.1$.

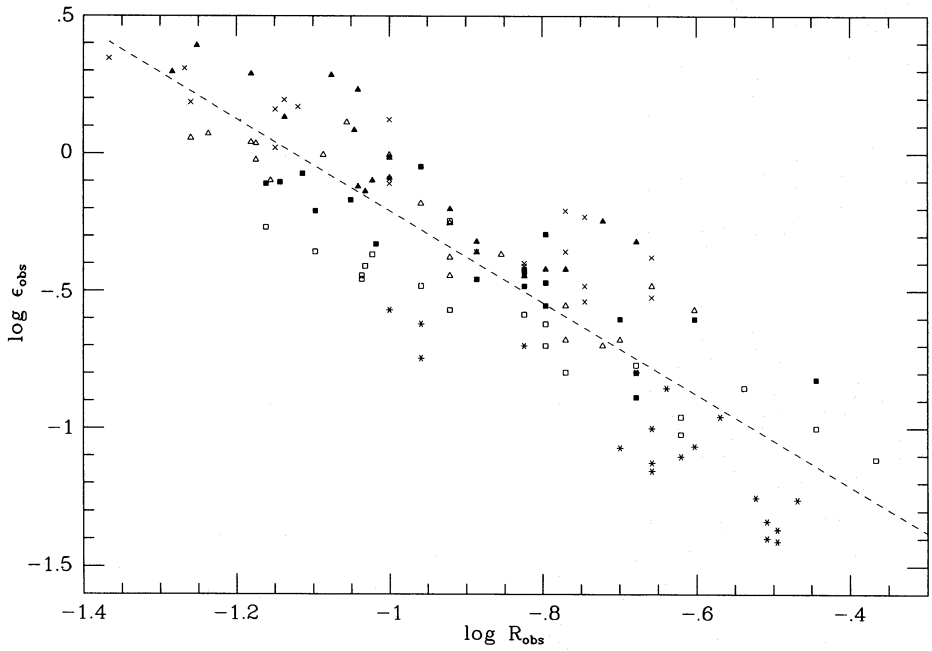

Figure A4. Log $\epsilon_{\rm obs}$ versus log $R_{\rm obs}$ for the simulated optically thin PN, where the symbols are the same as in Fig. A3. A least-squares fit to 120 points yields the following relation: $\log\epsilon_{\rm obs}=(-1.88\pm0.074)-(1.67\pm0.083)\log R_{\rm obs}$.

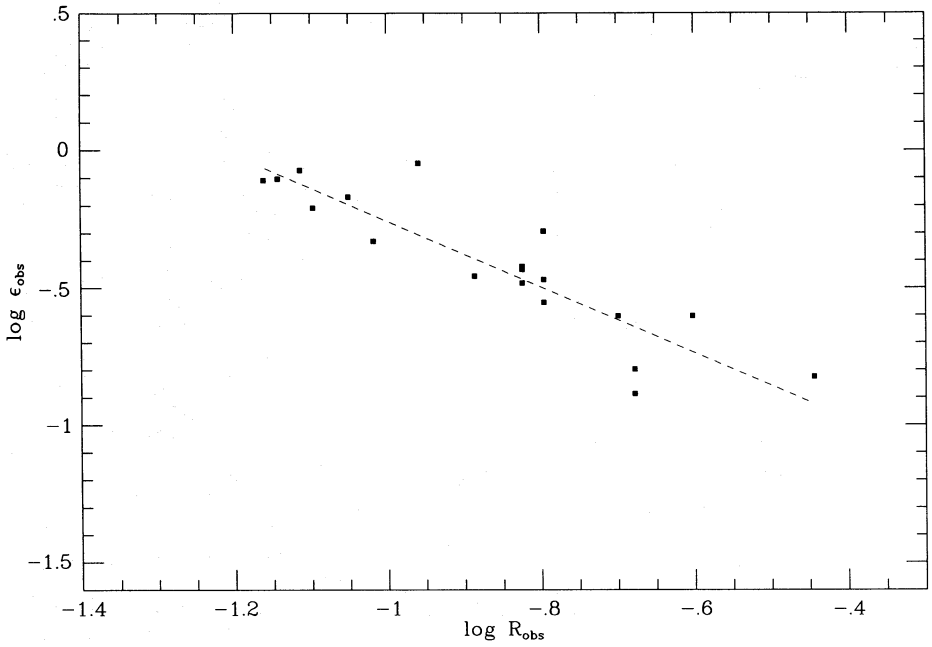

Figure A5. Log ϵ_{obs} versus log R_{obs} for simulated optically thin PN having only $\epsilon = 0.4$. A least-squares fit to the 20 points yields a slope of -1.20 ± 0.14.

this random number was made by generating another random number between 0 and 1; if this random number was <0.5 or >0.5, R was respectively divided or multiplied by the original random number to obtain R_{obs}. The derived values of R_{obs} were then used to evaluate 'observed' filling factors (ϵ_{obs}). Four sets of randomizations were performed for each value of ϵ, yielding 120 data points in all. Fig. A3 plots ϵ_{obs} versus R_{obs} and Fig. A4 presents the log of these quantities. We find a very similar distribution of points for these 'test' PN as seen in Figs A1 and A2. A least-squares fit to the 120 points in Fig. A4 yields a slope of -1.67 ± 0.083 with a correlation coefficient of -0.88. The slope obtained from Fig. A2, our observed values, is -2.62 ± 0.41. As only 14 points were used to derive this slope, we may say it is roughly consistent with that of our 'test' PN, and certainly the distributions of observed and 'test' points lie in the same range. Depending on the distance-scale sample they used, Mallik & Peimbert (1988) derived slopes ranging from -0.91 ± 0.18 to -1.38 ± 0.25.

One factor contributing to the slope found in Fig. A4 is that the 'test' PN with smaller ϵs are offset to larger radii compared to the 'test' PN with larger values of ϵ. In order to have a smaller ϵ at a given n_e(O II), a smaller n_e(rms), and hence a larger radius, is required. However, the 'test' PN with a single value of ϵ yield similar slopes to that found for the overall sample plotted in Fig. A4. For example, Fig. A5 plots log ϵ_{obs} versus log R_{obs} for $\epsilon = 0.4$ only. A least-squares fit to the 20 points in Fig. A5 yields a slope of -1.20 ± 0.14 and the mean ϵ_{obs} is 0.44 ± 0.25. The slopes for the 'test' PN with the five other values of ϵ ranged from -1.10 to -1.43.

In their 1988 paper, Mallik & Peimbert also proposed a new method for deriving distances to PN, based on an n_e(FL)–radius relation, where they found that $n_e(\mathrm{FL}) \propto R^{-0.96}$. However, examining our 'test' PN, we argue that such a relation again results because of the observational uncertainty associated with the adopted angular radius. A fit to log n_e(O II) versus log R_{obs} values for the 120 'test' PN points yields a slope of -0.50 ± 0.18, with a correlation coefficient of -0.24. The 20 'test' PN values obtained with $\epsilon = 0.4$ yield a slope of -0.61 ± 0.26. For the 14 optically thin PN in our observed sample, a slope of -0.05 ± 0.13 is found. Recalling that a slope of -3 is predicted theoretically, the observed deviation from this value appears to be consistent with uncertainties in the adopted angular diameters.

We therefore conclude that our present data provide no evidence for a physical relationship between the filling factor and the absolute nebular radius. A second paper (Kingsburgh & English, in preparation) will present new [O II] densities, distances and filling factors for a significant number of southern PN and should allow this conclusion to be tested for a larger sample.